DOE/ER/14180--1

DE92 005519

APPLICATION OF MAGNETOMECHANICAL HYSTERESIS MODELING TO MAGNETIC TECHNIQUES FOR MONITORING NEUTRON EMBRITTLEMENT AND BIAXIAL STRESS

PROGRESS REPORT
June 1991 – December 1991

M.J. Sablik, H. Kwun,
W.L. Rollwitz, and D. Cadena

Southwest Research Institute
San Antonio TX 78228-0510

January 1, 1992

PREPARED FOR THE U.S. DEPARTMENT OF ENERGY
UNDER GRANT NUMBER DE-FG05-91ER14180

ABSTRACT

The objective is to investigate experimentally and theoretically the effects of neutron embrittlement and biaxial stress on magnetic properties in steels, using various magnetic measurement techniques. Interaction between experiment and modeling should suggest efficient magnetic measurement procedures for determining neutron embrittlement and biaxial stress. This should ultimately assist in safety monitoring of nuclear power plants and of gas and oil pipelines.

In the first six months of this first year study, magnetic measurements were made on steel surveillance specimens from the Indian Point 2 and D.C. Cook 2 reactors. The specimens previously had been characterized by Charpy tests after specified neutron fluences. Measurements now included: (1) hysteresis loop measurement of coercive force, permeability and remanence, (2) Barkhausen noise amplitude; and (3) higher order nonlinear harmonic analysis of a 1 Hz magnetic excitation. Very good correlation of magnetic parameters with fluence and embrittlement was found for specimens from the Indian Point 2 reactor. The D.C. Cook 2 specimens, however, showed poor correlation. Possible contributing factors to this are: (1) metallurgical differences between D.C. Cook 2 and Indian Point 2 specimens; (2) statistical variations in embrittlement parameters for individual samples away from the stated mean values; and (3) conversion of the D.C. Cook 2 reactor to a low leakage core configuration in the middle of the period of surveillance. Modeling using a magnetomechanical hysteresis model has begun. The modeling will first focus on why Barkhausen noise and nonlinear harmonic amplitudes appear to be better indicators of embrittlement than the hysteresis loop parameters.

Table of Contents

LIST OF ILLUSTRATIONS

LIST OF TABLES

I. INTRODUCTION

This research project undertakes to investigate two areas of nondestructive evaluation (NDE) relating to safety in the energy industry:

1) the problem of nondestructively monitoring neutron embrittlement in nuclear pressure vessels; and

2) the problem of nondestructively detecting large stress levels in gas and oil pipeline, where both hoop and longitudinal stresses coexist in a biaxial stress condition.

These problems are important because of the need to insure that rupture of nuclear pressure vessels or of oil and gas pipeline does not occur. In the case of problem (1), the steel nuclear pressure vessel during operation is exposed to high energy (>1MeV) neutron irradiation, which over a long period of time eventually makes the steel very brittle and subject to rupture.[1] The need is to monitor the embrittlement nondestructively so that precautionary action can be taken when the vessel plates get embrittled enough that they should be taken out of service. In the case of problem (2), ground shifting, due to settling or due to freezing and thawing as in Alaska, can cause great stress in pipeline, enough to put it in danger of rupture.[2] Since pipeline is characterized by circumferential stress around the pipe and longitudinal stress along the pipe, the pipeline problem is one involving biaxial stress.

The approach in this project is to evaluate various magnetic NDE techniques as to their utility in monitoring the two conditions - neutron embrittlement and biaxial stress. This involves experimentally applying the magnetic NDE techniques to the conditions of interest and evaluating the detection sensitivity of the techniques. It also involves physical interpretation of the data based on

extension of the magnetomechanical hysteresis model[3-7] to the NDE techniques and conditions of interest. Development and use of the model will assist in better design of the techniques and in understanding how to use the detection methods to best advantage. It will also help explain why one technique might be more sensitive than another.

The magnetic NDE techniques[8-10] to be applied in this project are:

(1) magnetic hysteresis loop analysis;[3,10,11]

(2) nonlinear harmonics,[4,8,12-14] i.e. analysis of the fundamental and higher order harmonics of the hysteresis loop;

(3) Barkhausen noise analysis;[8,10,15-19]

(4) magnetically induced velocity change of ultrasonic waves (MIVC);[8,20-25]

(5) magabsorption;[6,9]

These techniques have all been used for residual stress measurements, though not necessarily for biaxial stress situations. Of these techniques, only (1), (3), and (5) have been used for studies of neutron irradiation damage. Regarding the latter, chiefly Barkhausen studies have been done.[26-29] Most of that work however has not been done on actual neutron-irradiated pressure vessel steel embrittled at temperatures corresponding to that of pressure vessel walls, viz. 550°F (290°C).[1,30-31] Preliminary studies of magabsorption monitoring of embrittled pressure vessel steels were completed many years ago at SwRI[29], which indicated a correlation between neutron embrittlement and magabsorption. Finally,

changes in hysteresis loop properties like coercivity[32], initial magnetization curve[32], permeability[33], and saturation remanence[34], have been studied for cases of neutron-damaged ferromagnetic specimens, not necessarily pressure vessel steel. An unreported study on Barkhausen studies of pressure vessel steel is presently ongoing in Britain.[35] Nevertheless, there have been few published studies on the utility of magnetic NDE techniques for monitoring reactor neutron-embrittled pressure vessel, and certainly none has been as comprehensive as our study will be.

The present report details work accomplished in the first six months of this research project. During this time the plan was to focus first on the neutron embrittlement problem. Hence, almost all of the work reported will pertain to the neutron embrittlement problem.

II. TECHNICAL DISCUSSION OF CHARPY TEST SPECIMENS USED IN NUCLEAR POWER PLANT SURVEILLANCE TESTING

At Southwest Research Institute, in a hot-cell facilitym there reside many Charpy test specimens obtained from neutron-irradiated capsules that had previously been inserted in various nuclear reactors around the country.

At reactor startup time, the encapsulated specimens are positioned inside the pressure vessel in the space between the pressure vessel wall and the thermal shield which surrounds the core region. (See Fig. 1).[31] The capsules are attached radially to the outer surface of the thermal shield rather than to the vessel surface, where fast neutron fluence is one-third less than at the shield. The capsules are immersed in water coolant at high pressure (>2000 psi) and high temperature (550°F, or equivalently, 290°C). The vertical position of the capsules is in the "beltline" region of the reactor intermediate between the top-most and bottom-most core region. (See Fig. 2)[1] A single capsule is removed during reactor shutdown service periods (spaced about 3 years apart). Specimens in each capsule are labeled by the number of effective full power years (EFPY) that the capsule was in service. A considerable number of dosimeters of different types are positioned inside the capsule along the entire length of capsule. These dosimeters plus the relative geometry of the fuel rods and capsule position allow the computation of average accumulated neutron irradiation per cm^2 or neutron fluence (in neutrons/cm^2) for each type of test specimen. Test specimens are typed by whether the specimen roll axis is parallel (Transverse (T) specimen) or perpendicular (Longitudinal (L) specimen) to the Charpy notch. (See Fig. 3 bottom right). In some cases, the specimens are also typed by relative position inside the capsule (i.e. at top, middle, or bottom of capsule, in which case they are labeled with different average fluences). Also, specimens are classified according to plates in the pressure vessel whether they

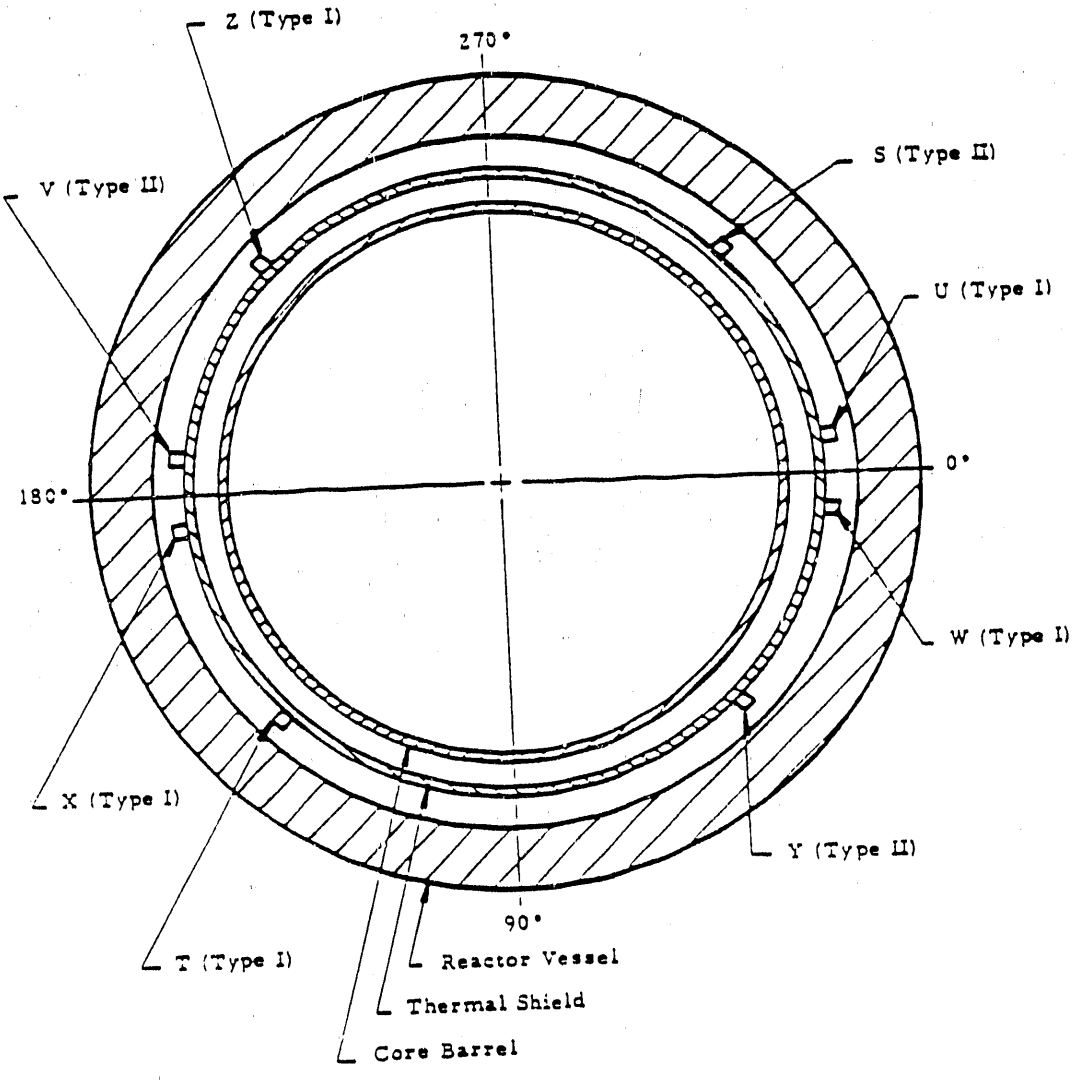

Fig. 1. Arrangement of surveillance capsules in a pressure vessel (after Ref. 32).

Fig. 2. Diagram of a pressurized water reactor (PWR). The beltline region is the region halfway down the length of the core region (after Ref. 31).

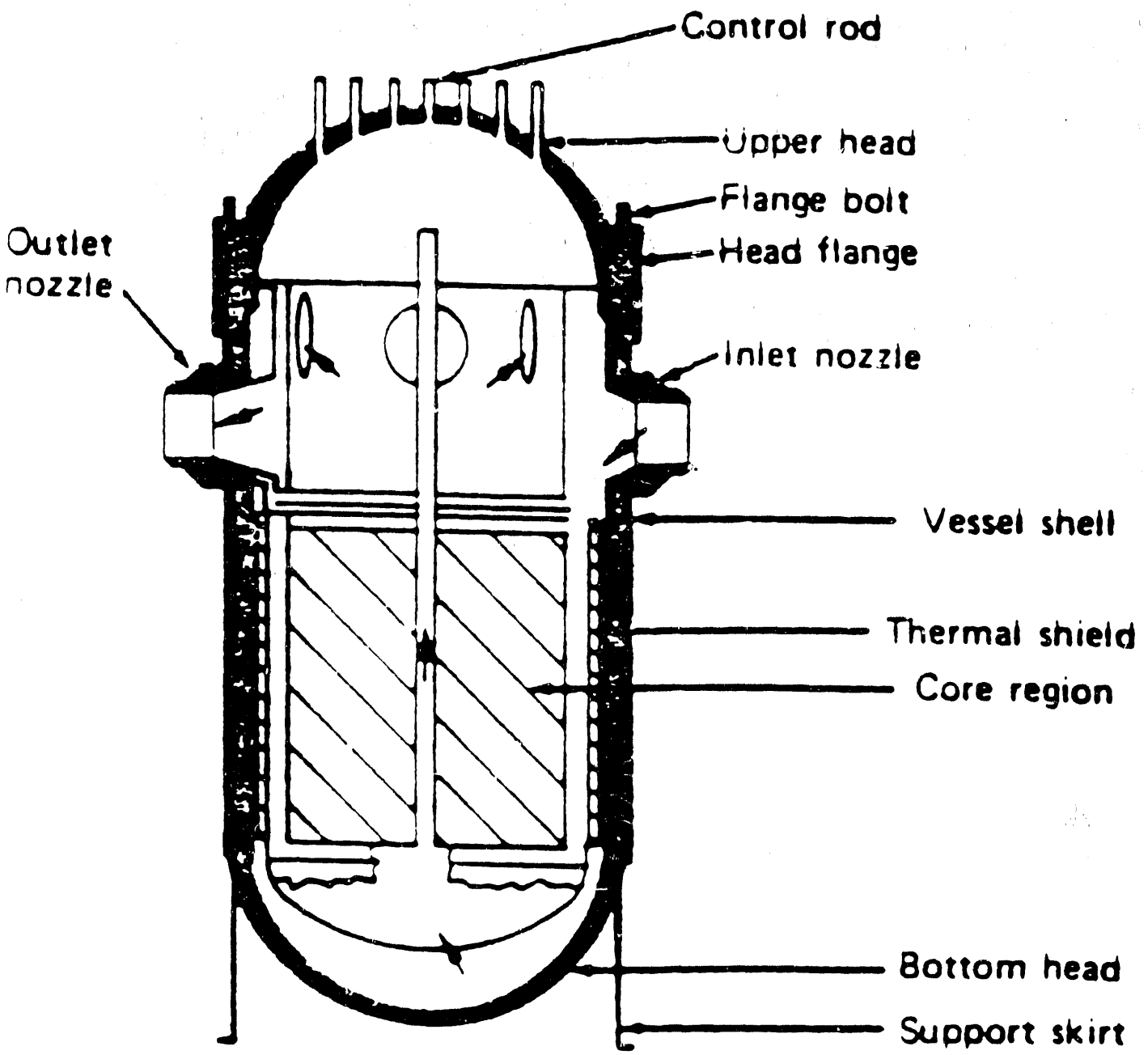

are plate specimens, specimens from welds similar to those between plates in the pressure vessel or whether they are from the heat affected zone surrounding a weld. We have used only plate specimens. Fluences are given only for fast neutrons with energies greater than 1MeV. Thus, neutron damage is correlated with fast neutron fluence, and not overall fluence including even thermal neutrons.

All the irradiated specimens stored at SwRI are destructively tested Charpy test specimens, which means that they have been broken in two after irradiation. Those under irradiation in a reactor capsule are unbroken. An unbroken Charpy test specimen is machined carefully according to ASTM specifications.[36] The unbroken specimens are 100 mm long with a square cross-section 10 mm on a side. The notch at mid-length is V-shaped at 45° and rounded to a 0.25 mm radius instead of coming to a point. Fig. 3, bottom right, shows the geometry.

The Charpy test is a standard ASTM test for degradation of the fracture toughness of the steels used. The Charpy specimen is placed in a Charpy rig. This means that the sample is put on an anvil and a specified weight mg is swung from a specified pendulum height h_o into the specimen in such a way that it hits the specimen when it is exactly vertical. The sample fractures, starting at the V notch. The energy given to the sample to break it is defined as its fracture toughness. This energy is measured by the height h_f to which the pendulum rises after it hits the sample, with the energy being given by $mg\ (h_o - h_f)$. If a steel sample has been irradiated with neutrons, its fracture toughness will have decreased depending on the amount of cumulative neutron fluence to which it has been exposed.

There are two types of fracture - ductile fracture and brittle fracture.[1,37] In the case of ductile fracture, the fracture usually involves necking and then tearing whereas in brittle fracture, the fracture is a crystallographic type of cleavage. At lower temperature, the fracture tends to be brittle fracture and at higher temperatures, the fracture is ductile fracture. The energy required for 100%

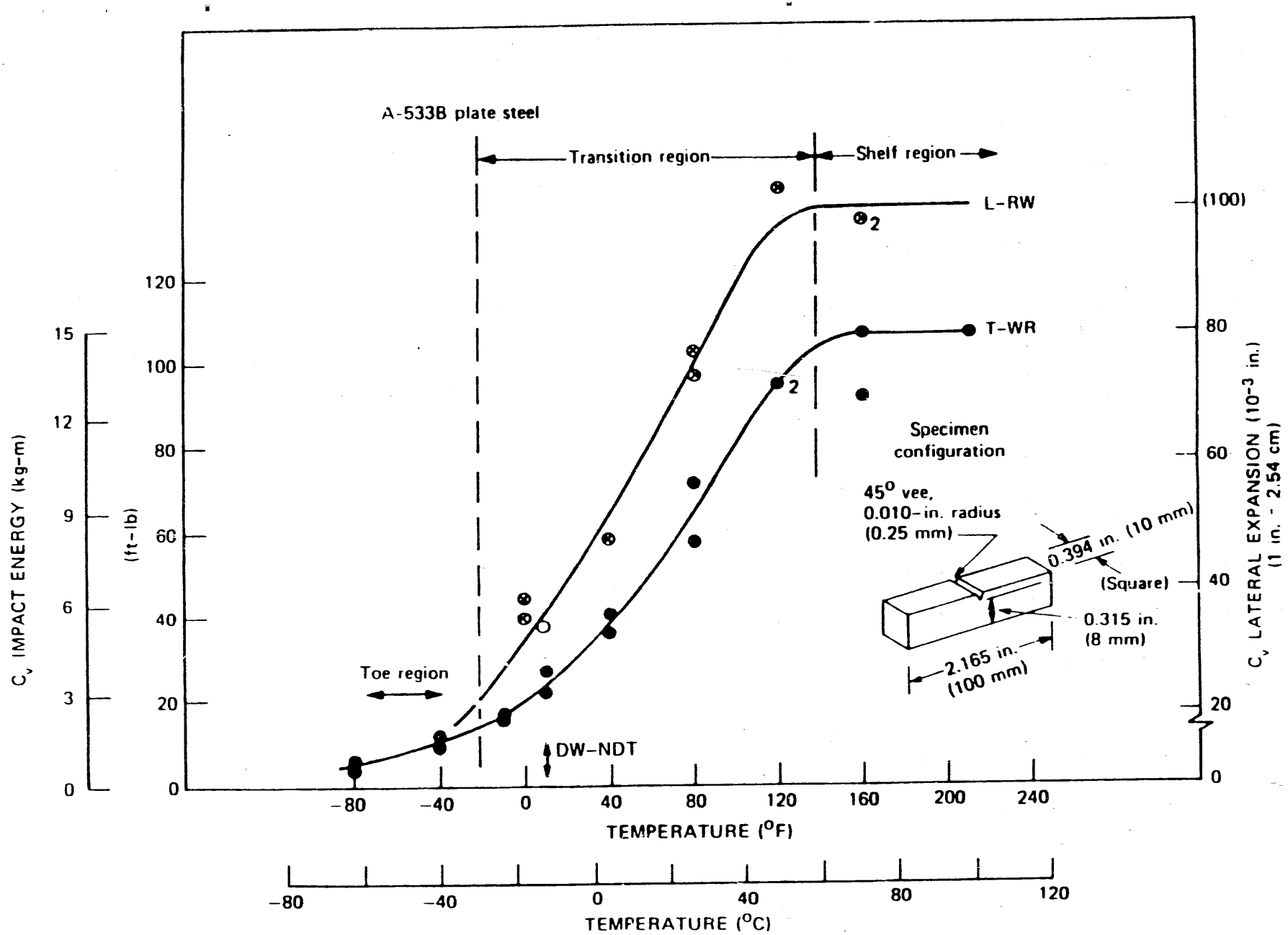

Fig. 3. Typical Charpy V-notch energy vs. temperature curves for A-533B plate steel showing orientation effects (L vs. T), the three regions of the transition curve, and a schematic view of the Charpy specimen design on the bottom right. (after Ref. 31).

ductile fracture is called the upper shelf energy, whereas the energy for 100% brittle fracture is the lower shelf energy. Neutron fluence has the effect of decreasing the upper shelf energy.[1,37] When both fracture toughness and upper shelf energy are decreased, the danger is that sudden fast rupture of the reactor pressure vessel is more likely and is a very present danger, particularly since the vessel contains hot, pressurized water.

Fig. 3 shows typical sets of Charpy data for specimens taken from a single capsule.[38] The data is for A-533B plate steel, typical of many reactor pressure vessels. The Charpy impact energy or fracture toughness (either in ft. - lb. or kg-m) is obtained for each Charpy sample from a specimen set, but where the temperature on impact for each sample is changed from sample to sample. The result is a curve which looks like a sloping step. The upper plateau of the curve at high temperatures corresponds to the upper shelf energy (needed for 100% ductile fracture). The two step-like curves shown in Fig. 3 are for transverse (T), and longitudinal (L) sample sets. Clearly, at a given temperature, it takes more energy to break a Charpy sample when the roll axis is perpendicular to the Charpy notch (L case). Note that the transition zone of mixed brittle-ductile fractures is fairly wide in terms of temperature or Charpy impact energy. Note too that is takes less energy to break a brittle specimen.

Fig. 4 shows how a Charpy curve changes after Charpy samples from the same batch of steel have been irradiated, in this case to 3 x 10^{19} n/cm^2 of fluence.[39] The tendency is for the transition region to shift to higher temperatures (making the samples more brittle at a given temperature); also the upper shelf energy tends to decrease (requiring less energy for ductile fracture). One parameter that can be used as a measure of neutron embrittlement is the temperature shift of the Charpy curve at a given energy (taken by ASTM standards to be 60 ft-lb, which is roughly the energy for 50% brittle - 50% ductile fracture). The temperature shift at 60 ft.-lbs is usually designated as ΔT_{NDT} or RT_{NDT}. (NDT stands for "nil ductility temperature" or the temperature at which ductile fracture is expected to

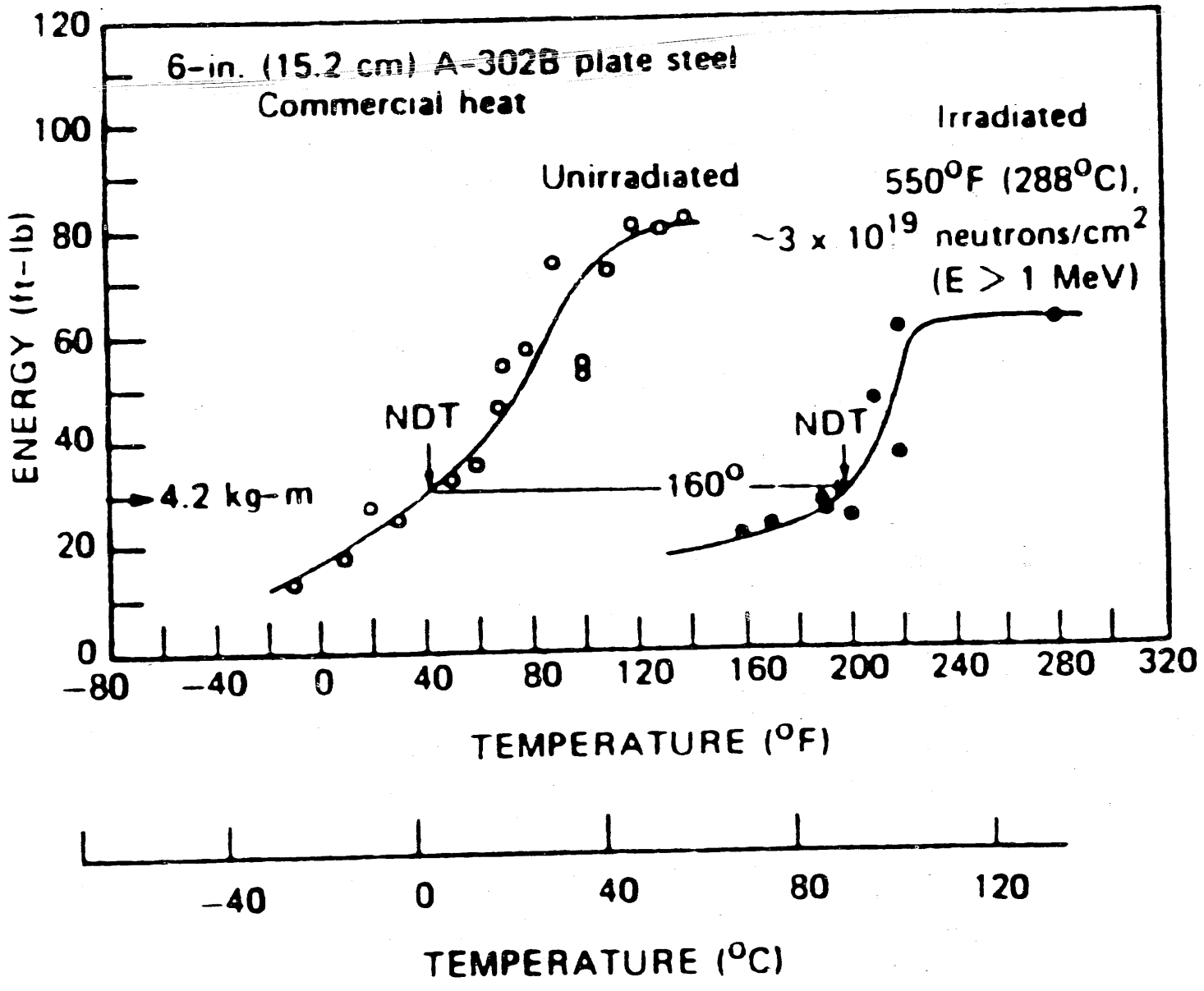

Fig. 4. Typical Charpy V impact data for irradiated A-302B plate steel. (after Ref. 31).

no longer dominate; R stands for "reference" and refers to temperature shift at the reference energy corresponding to 60 ft-lb.) Another parameter that can be used as a measure of embrittlement is the change in the upper shelf energy (Δ(USE)), which measures ease of ductile fracture at the higher temperatures. As the upper shelf energy shifts to lower energies after more and more irradiation, it is seen that the change Δ(USE) gets larger.

III EXPERIMENTAL DESCRIPTION

A. Specimens

Table 1 shows Charpy data and average mechanical properties for SwRI Charpy specimens taken from the Indian Point Unit 2 reactor. Table 2 shows the same type of data for D.C. Cook Unit 1 and D.C. Cook Unit 2 reactors. The Charpy data in the tables are also plotted in Figs. 5 and 6. Points 1, 2, and 3 are data corresponding to plate specimens 2002-1, 2002-2, and 2002-3 from Indian Point Unit 2; points L and T correspond to longitudinal and transverse specimens from D.C. Cook Unit 1; points A and B correspond to longitudinal and transverse specimens from D.C. Cook Unit 2.

Fig. 5 is a plot of ΔT_{NDT} vs. neutron fluence, using data from the various reactors. Except for the 2 point from capsule V at Indian Point Unit 2, the data generally shows a monotonic increase with fluence. Point 2 is obviously an exception since its fluence is small and its effective full power years (EFPY) are large, suggesting that perhaps due to its geometric position in the reactor, some of the faster neutrons may have been screened out, thereby decreasing the neutron damage. In fact point 2 was from a capsule which was designed to get a more screened exposure, corresponding to that seen by the pressure vessel itself. It is also noted that whereas data points 3 from Indian Point shows a roughly linear increase with fluence, the D.C. Cook data tends to level off quite dramatically for points with the largest fluence. It was later determined that between the second and third capsule for both D.C. Cook units, a low leakage core configuration was installed, screening off the much faster neutrons from the capsule, thereby decreasing embrittlement changes for the same amount of total fluence for neutron energies greater than 1 MeV.

Fig. 6 is a plot of change in upper shelf energy vs. neutron fluence, again using data from the various reactors. In general, upper shelf energy does not correlate as well with fluence as transition temperature shift ΔT_{NDT}, but nevertheless similar trends are seen in this data as were seen in

TABLE 1. Indian Point 2 Reactor Data on Charpy Specimens

Capsule	*EFPY*	*Plate*	*Fluence*	*Δ(USE) Ft-Lbs*	*ΔT_{NDT} °C*	*.2% YS*	*Tensile Test Temp.*	*Young's Modulus*
T	1.42	2002-1	$2.93X10^{18}$	15	60	71.1	550	32.0
		2002-2	$2.93X10^{18}$	11	95	58.6	550	33.5
		2002-3	$2.55X10^{18}$	22	120	63.1	550	29.3
Y	2.34	2002-3	$4.72X10^{18}$	32.5	145	76.4	550	28.7
		2002-3	$4.72X10^{18}$	—	—	—	550	35.0
Z	5.17	2002-1	$1.2X10^{19}$	25	130	81.6	300	22.9
		2002-2	$1.2X10^{19}$	27	120	69.9	300	24.96
		2002-3	$9.6X10^{18}$	32	185	74.3	300	22.6
V	8.6	2002-2	$4.57X10^{18}$	6	80	65.3	75	25.5
		2002-2	$4.57X10^{18}$	—	—		550	18.5

TABLE 2. D.C. Cook Reactor Data on Charpy Specimens

Capsule	*EFPY*	*Plate*	*Fluence*	*Δ(USE) Ft-Lbs*	*ΔT_{NDT} °C*	*.2% YS*	*Tensile Test Temp.*	*Young's Modulus*
DC Cook Unit 1								
T	1.13	4406-3L	$1.8X10^{18}$	17	75	72.7	84	33.4
		4406-3L	$1.8X10^{18}$	—	—	—	550	37.0
		4406-3T	$1.8X10^{18}$	11	75	86.1		
X	3.48	4406-3L	$7.7X10^{18}$	28	110			
		4406-3T	$6.2X10^{18}$	17	110	77.7	250	32.8
		4406-3T	$6.2X10^{18}$	—	—		550	28.3
Y	4.94	4406-3L	$1.34X10^{19}$	26	120	72.7	250	34.9
		4406-3L	$1.34X10^{19}$	—	—	—	550	25.0
		4406-3T	$1.06X10^{19}$	18	115	73.4		
DC Cook Unit 2 (2L →A, 2T→B)								
T	1.08	C5521-2L	$2.3X10^{18}$	16	55			
		C5521-2T	$2.3X10^{18}$	12	80	58.7	250	33.3
		C5521-2T	$2.3X10^{18}$	—	—		550	25.7
Y	3.24	5521-2L	$7.01X10^{18}$	24	90			
		5521-2T	$7.01X10^{18}$	18	100	72	210	27.5
		5521-2T	$7.01X10^{18}$	—	—		550	27.4
X	5.27	5521-2L	$1.0X10^{19}$	42	95			
		5521-2T	$1.0X10^{19}$	23	103	76	250	22.5
		5521-2T	$1.0X10^{19}$	—	—		550	28.3

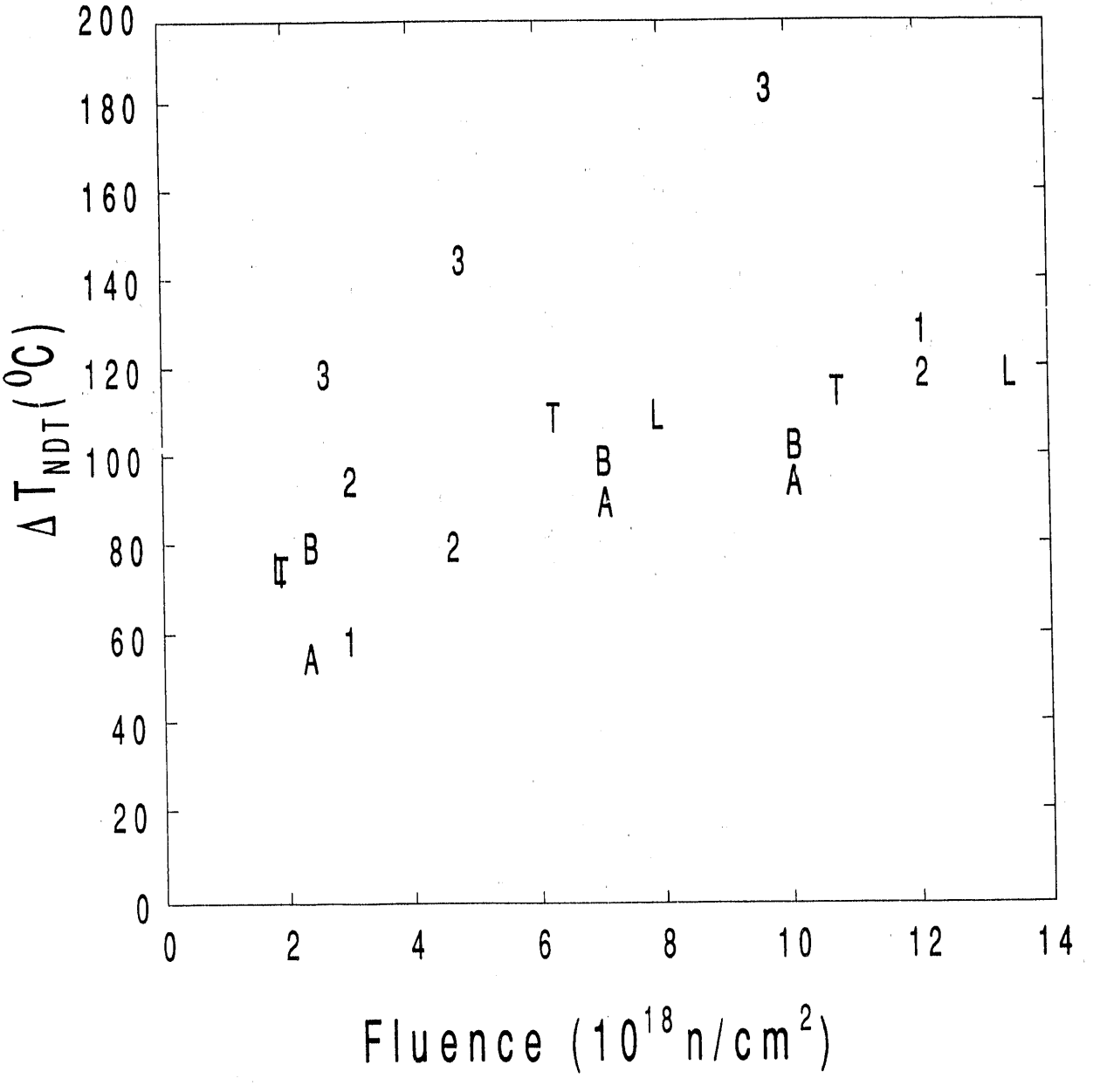

Fig. 5. Transition temperature shift ΔT_{NDT} vs. neutron fluence for specimens in Tables 1 and 2. L and T refer to longitudinal and transverse specimens for the D.C. Cook 1 reactor and A and B refer to longitudinal and transverse specimens for the D.C. Cook 2 reactor. 1, 2, and 3 refers to specimens from the Indian Point 2 reactor.

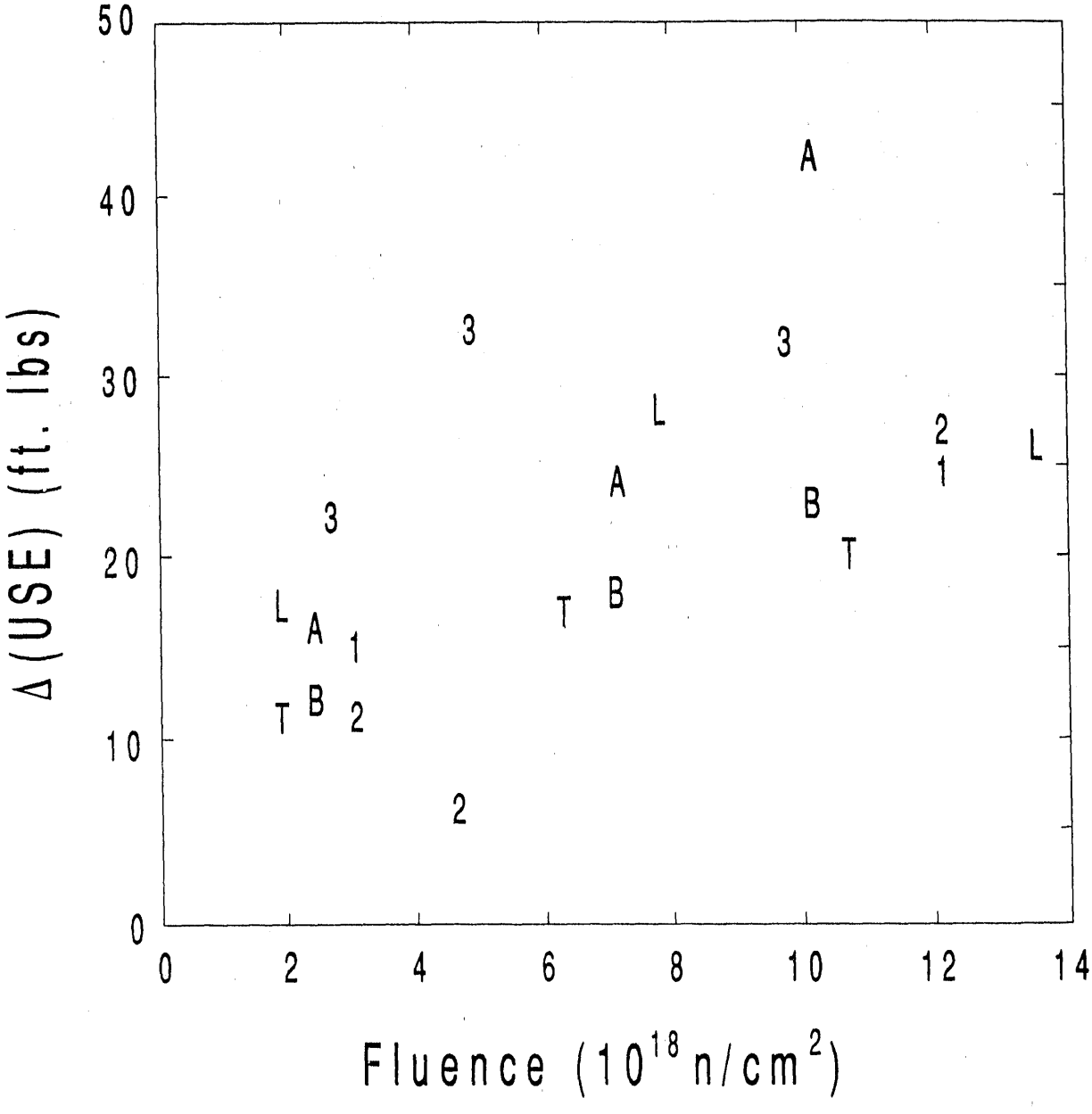

Fig. 6. Change in upper shelf energy Δ(USE) vs. neutron fluence for specimens described in Tables 1 and 2. L, T, A, B, 1, 2, and 3 are defined as in Fig. 5.

Fig. 5.

According to an analysis performed by D.G. Cadena, the experimental accuracy for the data in Table 1 for the Indian Point 2 reactor is estimated to be ± 5° in ΔT_{NDT} and ± 4 ft.-lbs in change in upper shelf energy. The experimental accuracy for the D.C. Cook data is ± 5° in ΔT_{NDT} and ± 5 ft.-lbs in change in upper shelf energy. Fluences are known to within ± 5%. It should be pointed out however that the error estimates refer to error in the mean of a group of samples, and not the error in the value for a specific sample to which the mean value is assigned. Dosimetry analysis is performed according to a standard dosimetry analysis computer calculation.[40]

Table 3 and Table 4 show the specimen chemical compositions and heat treatments for the Indian Point 2 and D.C. Cook 2 reactors respectively. Differences in chemical composition occur chiefly in sulfur, silicon, copper and chromium content. The Indian Point 2 plate steel is classified as a modified SA 302 Grade B steel, whereas D.C. Cook 2 steel is also classified as SA533 Grade B steel. The heat treatments also differ slightly, with the D.C. Cook 2 steel receiving an extra period at high temperatures followed by water quenching. The stress-relief period was also longer for the D.C. Cook 2 steel.

It was decided that test specimens corresponding to points 3 from Indian Point 2 be used for the magnetic measurements. It was also decided that specimens corresponding to points A (longitudinal specimens) from D.C. Cook 2 be also used for the magnetic measurements. Again, these are broken Charpy specimens and hence are half the length depicted in Fig. 3.

TABLE 3. Indian Point Unit No. 2 Pressure Vessel Plate Metallurgical Data

Combustion Engineering, Inc., furnished sections from three hot-formed 9-5/8" thick plates (B2002-1, B2002-2, and B2002-3) of SA 302 Grade B modified steel and a weldment joining two formed plates (B2002-1 and B2002-3) used in the fabrication of the Indian Point Unit No. 2 reactor pressure vessel intermediate shell course. These plates were produced by the Lukens Steel Company.

a. Chemical Analyses (Percent)

Plate No.	Lukens Heat No.	C	Mn	P	S	Si	Ni	Mo
B2002-1	B4688-2	0.20	1.28	0.010	0.019	0.25	0.58	0.46
B2002-2	B4701-2	0.22	1.30	0.014	0.020	0.22	0.46	0.50
B2002-3	B4922-1	0.22	1.29	0.011	0.018	0.25	0.57	0.46

b. Heat Treatment

The sections of formed shell plate material were heat treated by Combustion Engineering as follows:

1550° – 1650°F, 4 hours, Water Quenched

1225° ± 25°F, 4 hours, Air Cooled

1150° ± 25°F, 40 hours, Furnace Cooled to 600°F

The weldment was stress-relieved by Westinghouse as follows:

1150° ± 25°F, 19-3/4 hours, Furnace Cooled to 600°F

TABLE 4. Donald C. Cook Unit No. 2 Reactor Vessel Surveillance Materials

Heat Treatment History

Shell Plate Material:

Heated to 1700°F for 4-1/2 hours, water quenched.

Heated to 1600°F for 5 hours, water quenched.

Tempered at 1250°F for 4-1/2 hours, air cooled.

Stress relieved at 1150°F for 51-1/2 hours, furnace cooled.

Weldment:

Stress relieved at 1140°F for 9 hours, furnace cooled.

Chemical Composition (Percent)

Material	C	Mn	P	S	S1	N1	Mo	Cu	Cr
Plate C-5521-2[a]	0.21	1.29	0.013	0.015	0.16	0.58	0.50	0.14	— –
Plate C-5521-2[b]	0.22	1.28	0.017	0.014	0.27	0.58	0.55	0.11	0.072
Weld Metal[b]	0.11	1.33	0.022	0.012	0.44	0.97	0.545	0.055	0.068
Weld Metal[c]	0.08	1.42	0.019	0.016	0.36	0.96	—	0.05	0.07

(a) Lukens Steel analysis.
(b) Westinghouse analysis.
(c) Chicago Bridge and Iron analysis.

B. Experimental Setup and Instrumentation for Measuring Magnetic Hysteresis, Nonlinear Harmonics, and Barkhausen Noise

So far, only techniques (1) - (3) (See Introduction) of the magnetic NDE techniques have been used for measurements on the Charpy specimens. A magabsorption setup (technique (5)) is presently being designed for the available specimen size . An MIVC setup (technique (4)) will be configured for measurements in the early portion of 1992.

Before any measurements were started with radioactive Charpy specimens, a radiation safety class was held for all technicians and professionals on the project who would be involved with measurements on the radioactive specimens. The class was taught by D.G. Cadena, Jr., radiation safety officer of the Institute. The class dealt with precautions to be taken before and while conducting such experiments.

Measurements of (1) magnetic hysteresis parameters, (2) nonlinear harmonics, and (3) Barkhausen noise were made with the appropriate instrumentation using a common magnetization arrangement and sensors. A block diagram of the magnetization and sensor arrangement and the instrumentation is shown in Figure 7 and a photograph of the actual setup is shown in Figure 8. A magnetizing coil and magnetic circuit were used to magnetize the specimens. The applied magnetic field was measured with a Hall - effect sensor placed on the surface of the specimen; and the magnetic induction in the specimen, the nonlinear harmonics, and the Barkhausen noise (BN) were measured using an encircling sensing coil. The sensing coil was wound on a plastic coil form which could be slipped over each specimen, and a plastic fixture was used to position both the sensing coil and the specimens in the magnetic circuit.

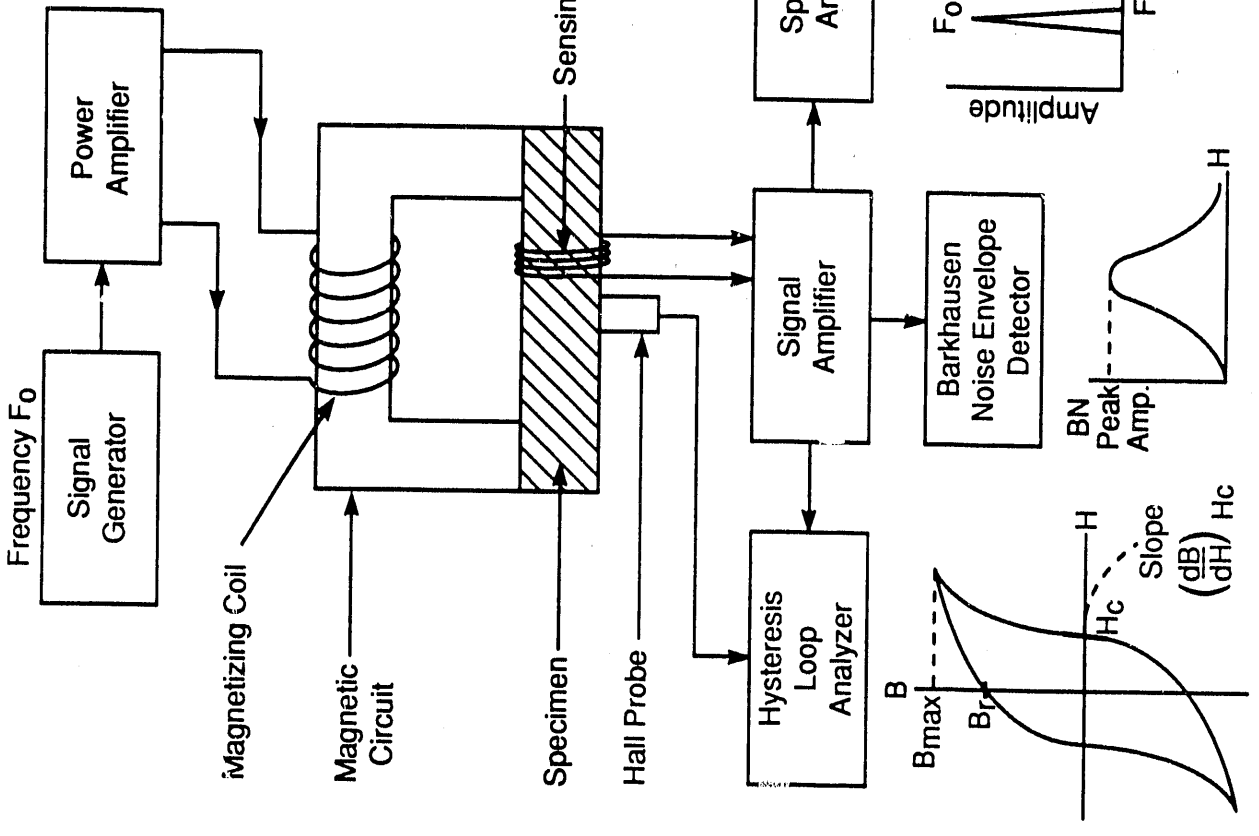

Fig. 7. Sensor and instrumentation arrangement for magnetic hysteresis, nonlinear harmonics, and Barkhausen noise measurements.

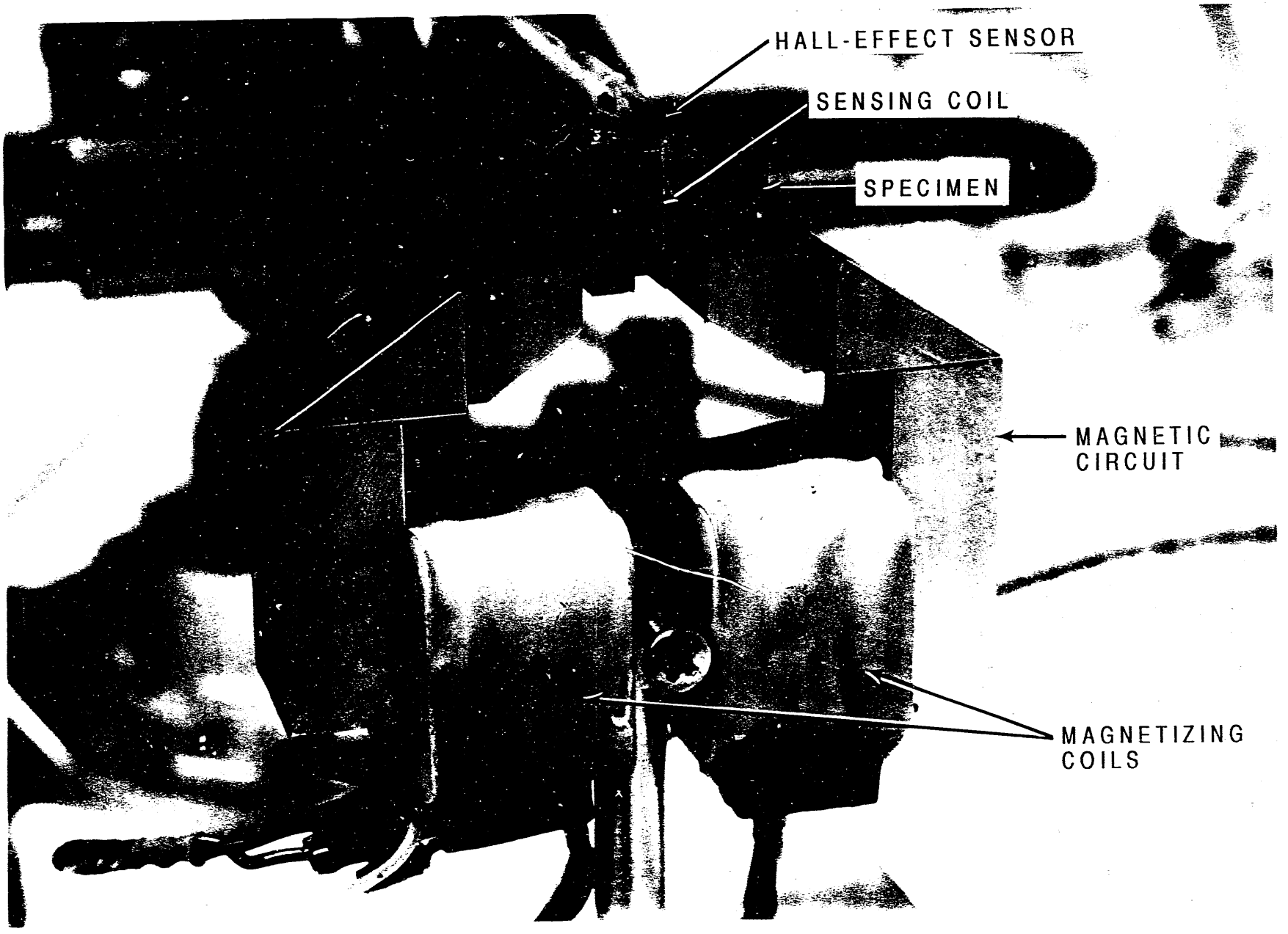

Fig. 8. Photograph of magnetic circuit, sensors, and specimen. A plastic fixture, not shown in the photograph, was used to precisely position the specimen into the magnetic circuit.

A signal generator and power amplifier were used to drive the magnetizing coil. A sinusoidal waveform at a frequency of 1 Hz was used for the hysteresis loop and nonlinear harmonics measurements, and a triangular waveform at a frequency of 0.5 Hz was used for the BN measurements (the triangular waveform provides a linear change of the applied magnetic field in the region where Barkhausen noise is generated.) The signal from the sensing coil is amplified and then directed to (1) a spectrum analyzer for measuring the harmonics, (2) a Barkhausen noise system which generates a signal proportional to the envelope of the Barkhausen noise burst and measures the peak amplitude of the envelope, and (3) a hysteresis loop analyzer which generates the hysteresis loops from the sensing coil and Hall-effect sensor signals and determines the magnetic parameters from the loop generated.

Using the instrumentation illustrated in Figure 7, eight magnetic parameters listed in Table 5 were measured from each sample. Except for Barkhausen noise peak amplitude, all the parameters were measured at four different levels of H_{max} to evaluate whether the magnetization level affects the correlations between the magnetic parameters and the fluence, change in upper shelf energy, and ΔT_{NDT}. The approximate values of the applied H_{max} were, respectively, level 1 - 8 Oe, level 2 - 16 Oe, level 3 - 27 Oe, and level 4 - 48 Oe. All samples showed a magnetic saturation at H_{max} level 4.

Five repeat-measurements were carried out using an unirradiated SA533B specimen obtained from Babcock and Wilcox. In each measurement, the sample was taken out of the plastic fixture and then repositioned. The measurement error (100% x standard deviation/mean) of the experimental setup and instrumentation was then determined based on these measurements and is given in Table 5. The error values in the table represent those determined at H_{max} level 1. At higher H_{max} level, the error was proportionally smaller; it was reduced to approximately 1/3 of those given in the table at level 4. Except for the parameter dB/dH at H_c, the measurement error was within a few percent.

TABLE 5. Magnetic Parameters and Their Measurement Error

No.	*Magnetic Parameter*	*Measurement Error (%)*
1	F_0 — Fundamental Frequency Amplitude	+/- 0.9
2	$F_3 = 3F_0$ — Third Harmonic Amplitude	+/ · 1.4
3	$F_5 = 5F_0$ — Fifth Harmonic Amplitude	+/- 1.5
4	H_c / H_{max}	+/- 3.1
5	B_r / B_{max}	+/- 1.7
6	B_{max} / H_{max}	+/- 3.6
7	dB / dH at H_c	+/- 11.4
8	Barkhausen Noise Peak Amplitude	+/- 0.8

In determining the hysteresis loop parameters, only one loop cycled at 1 Hz was actually digitized and all hysteresis loop parameters such as H_c/H_{max}, B_r/B_{max}, B_{max}/H_{max}, and dB/dH at H_c were extracted from this one loop for each specimen and H_{max} level. (A better procedure would have been to average the parameters from 4 digitized loops per specimen and H_{max} level. This would tend to reduce experimental error by a factor of 2.)

The harmonic amplitudes were read digitally from the spectrum analyzer. The Barkhausen noise amplitudes were also read digitally by the Barkhausen noise system.

All of the digitized information was tabularized by an internal computer program and outputted as a separate line in the table for each sample and each H_{max} level.

C. Experimental Results and Discussion

The digitized data obtained from hysteresis loops and the corresponding nonlinear harmonic and Barkhausen noise (BN) measurement was evaluated using statistical techniques in order to determine how well they were related to fluence, change in upper shelf energy, and ΔT_{NDT} (transition temperature shift). The R^2 value, which is the square of the correlation coefficient (see Appendix 1), was determined for each parameter as a measure of this relationship, and the results are shown in Table 6. The R values of + or - 1 indicate perfect correlation with positive and negative slopes of the fit respectively, and the correlation decreases as the R values approach 0, with a 0 value indicating no correlation. Note that 7 of the magnetic parameters were measured at 4 different magnetization levels; for BN, only one magnetization level was used.

Good correlation was obtained with fluence and ΔT_{NDT} for several of the magnetic

TABLE 6. Square of Correlation Coefficient (R^2) for Measured Magnetic Parameters

		Indian Point			*DC Cook Unit 2*		
	Field Level	*Fluence*	*Δ(USE)*	*ΔT_{NDT}*	*Fluence*	*Δ(USE)*	*ΔT_{NDT}*
Barkhausen Noise	—	0.89	0.69	0.92	0.13	0.09	0.15
Fund. Amp	H_{max} 1	0.93	0.51	0.93	0.00	0.00	0.00
	H_{max} 2	0.86	0.58	0.88	0.03	0.03	0.02
	H_{max} 3	0.74	0.44	0.74	0.15	0.20	0.10
	H_{max} 4	0.30	0.11	0.29	0.43	0.62	0.24
3rd Har. Amp.	H_{max} 1	0.94	0.54	0.95	0.02	0.04	0.01
	H_{max} 2	0.95	0.61	0.97	0.00	0.00	0.00
	H_{max} 3	0.92	0.64	0.94	0.00	0.00	0.00
	H_{max} 4	0.90	0.61	0.92	0.04	0.04	0.03
5th Har. Amp.	H_{max} 1	0.86	0.63	0.88	0.03	0.07	0.00
	H_{max} 2	0.99	0.51	0.99	0.00	0.01	0.00
	H_{max} 3	0.95	0.63	0.87	0.00	0.00	0.00
	H_{max} 4	0.91	0.64	0.93	0.03	0.03	0.02
H_c / H_{max}	H_{max} 1	0.01	0.21	0.02	0.12	0.15	0.08
	H_{max} 2	0.13	0.03	0.09	0.16	0.18	0.12
	H_{max} 3	0.00	0.39	0.00	0.37	0.45	0.25
	H_{max} 4	0.36	0.77	0.42	0.41	0.64	0.21
B_r / B_{max}	H_{max} 1	0.81	0.47	0.81	0.00	0.00	0.01
	H_{max} 2	0.72	0.59	0.75	0.00	0.00	0.00
	H_{max} 3	0.59	0.51	0.61	0.00	0.00	0.01
	H_{max} 4	0.61	0.69	0.65	0.01	0.01	0.01
B_{max} / H_{max}	H_{max} 1	0.65	0.54	0.70	0.01	0.01	0.00
	H_{max} 2	0.15	0.01	0.11	0.12	0.10	0.12
	H_{max} 3	0.37	0.00	0.31	0.18	0.15	0.17
	H_{max} 4	0.28	0.01	0.21	0.39	0.47	0.28
$\frac{dB}{dH}$ at Hc	H_{max} 1	0.09	0.06	0.09	0.01	0.00	0.01
	H_{max} 2	0.04	0.19	0.05	0.56	0.57	0.45
	H_{max} 3	0.15	0.13	0.15	0.00	0.02	0.04
	H_{max} 4	0.50	0.35	0.52	0.16	0.11	0.18

parameters for the Indian Point specimens, and moderate correlation was obtained for the upper shelf energy. The best results were obtained from the BN, and 3rd and 5th harmonic amplitudes, all of which had R^2 values ranging from a minimum of 0.88 to a maximum of 0.99 for ΔT_{NDT} and from 0.86 to 0.99 for fluence. The upper shelf energy values for these parameters were lower and ranged from 0.51 to 0.69. No clear trend in the correlation was observed for the different applied magnetic field levels (H_{max}) for these parameters, thus indicating that only one H_{max} value may be needed for future measurements.

Typical results for the Indian Point specimens are illustrated in Figures 9, 10, and 11. These plots show the 3rd harmonic signal amplitude (H_{max} level 2) vs. fluence, upper shelf energy, and ΔT_{NDT}; the corresponding R^2 values are 0.95, 0.61 and 0.97 respectively. The 3rd harmonic increases with increasing fluence and ΔT_{NDT} and although some scatter exists in the 3rd harmonic value, there is good separation between the groups of 3rd harmonic values at each of the 3 values of fluence and ΔT_{NDT}. The plot of the 3rd harmonic vs. upper shelf energy (Figure 11) did not show as good of a relationship as did the fluence and ΔT_{NDT}; the 3rd harmonic increased with increasing energy and then decreased somewhat. The upper shelf energy change, however, did not consistently increase with increasing fluence, as did ΔT_{NDT}. The three groups of specimens had energy values of 22, 32.5, and 32, corresponding to fluence values of 2.55, 4.72, and 9.6×10^{18} and ΔT_{NDT} values of 120°, 145°, and 185° respectively. If the upper shelf energy change had increased with increasing fluence, thus having the effect of reversing the last 2 energy values in the plot in Figure 11, the 3rd harmonic would have increased monotonically with increasing Δ(USE). It appears that the inconsistent behavior of the magnetic techniques with upper shelf energy change may be caused by the inconsistent relationship between the energy value and the fluence.

The response of the magnetic techniques to the specimens from the D.C. Cook 2 reactor did not correlate well with the fluence, upper shelf energy, or T_{NDT}. The R^2 values (Table 6) are very

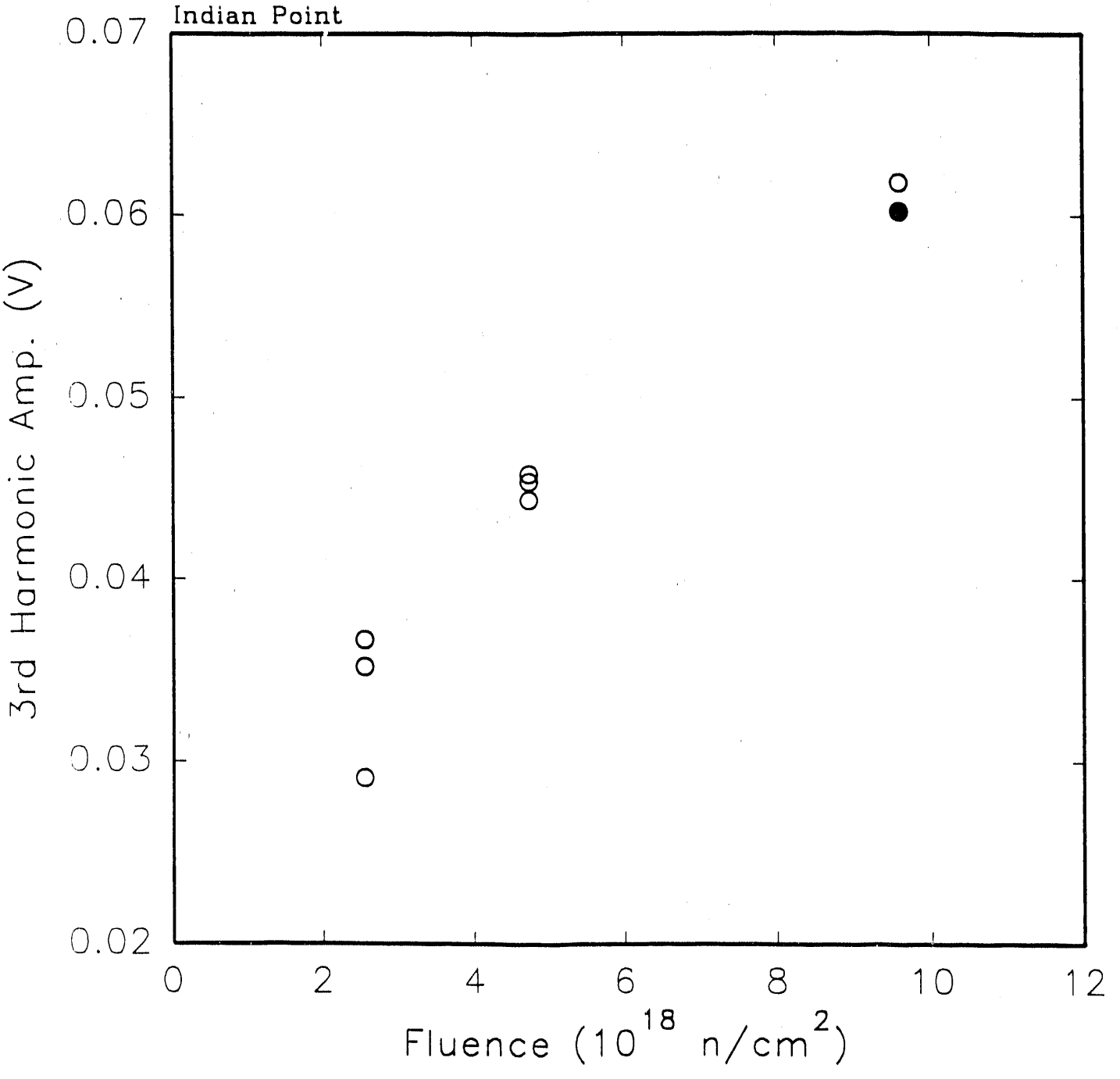

Fig. 9. Scatter plot for third harmonic signal amplitude (H_{max} level 2) vs. fluence for Indian Point 2 reactor. The dark circle indicates the coincidence of two open circle points.

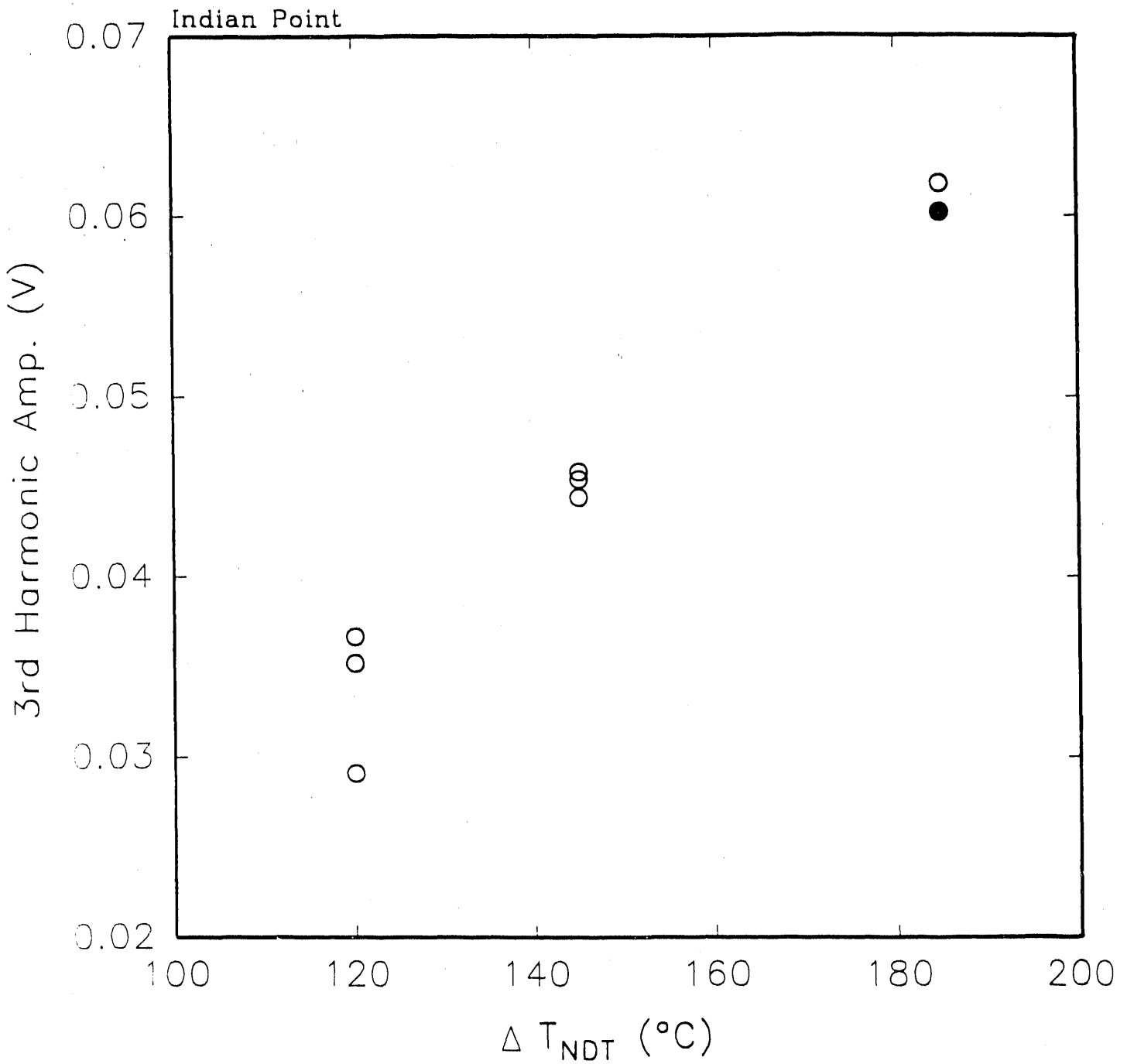

Fig. 10. Scatter plot for third harmonic signal amplitude (H_{max} level 2) vs. transition temperature shift ΔT_{NDT} for Indian Point 2 reactor.

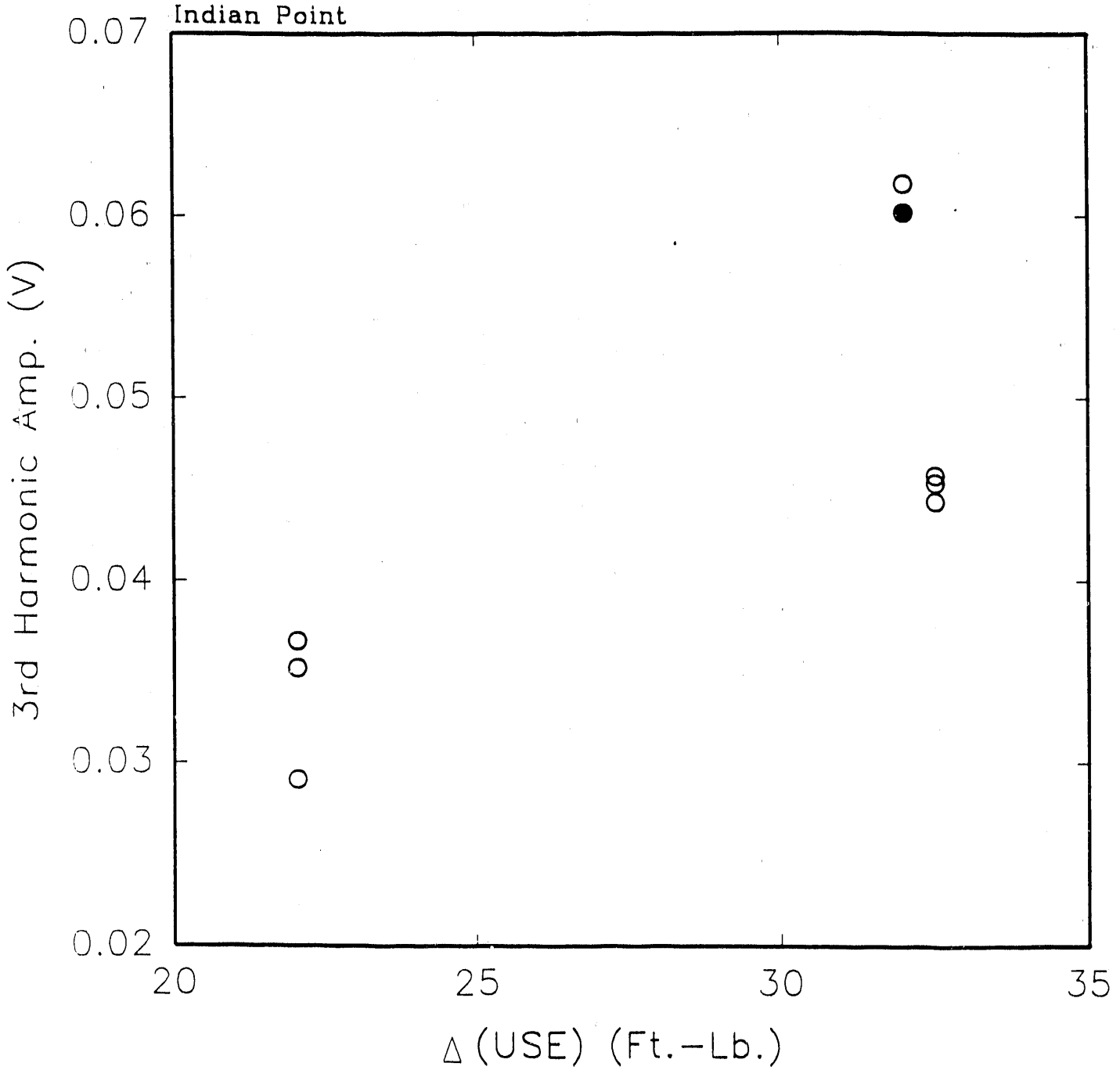

Fig. 11. Scatter plot for third harmonic signal amplitude (H_{max} level 2) vs. change Δ(USE) in upper shelf energy for Indian Point 2 reactor.

low (in some cases 0) for all of the magnetic parameters. Typical data are shown in Figures 12, 13, and 14 which are plots of the third harmonic (magnetization level 2) vs. fluence, upper shelf energy, and ΔT_{NDT}; the R^2 values are 0 for all 3 parameters. (In contrast, the 3rd harmonic amplitude produced the best results for the Indian Point specimens). In all three plots, there is no discernable trend in the data compared to the degree of scatter in the 3rd harmonic values. Since the scatter in the data was significantly greater than the experimental measurement error discussed in Section II B, it is believed that the scatter represents the actual variation in the sample properties. Also, the change in the remaining magnetic parameters caused by the irradiation appears to be comparable to the measurement error, thus resulting in a very low R^2 value.

Possible reasons for the inconsistent behavior for the D.C. Cook 2 data, as compared to the Indian Point 2 data, include differences in chemical composition and heat treatment, which might result in lower levels of embrittlement. (Compare points 3 and points L in Figs. 5 and 6.) More importantly, such differences could also result in reduction of sensitivity of the magnetic parameters to embrittlement. Thus, for example, magnetic parameters for Indian Point 2 specimens show changes which are three to four times as large that found for corresponding D.C. Cook 2 specimens. When experimental error is added into consideration, one might expect D.C. Cook 2 specimens to have magnetic parameters which show dramatically less correlation with fluence and embrittlement parameters.

Another point is that all the samples from a particular set of samples at a given fluence are assigned the same value of ΔT_{NDT} and Δ(USE), even though their individual embrittlements may actually differ in nature. The result is that the embrittlement factors that are assigned to individual samples should have a larger error in them than that assigned to the mean for the group. This is corroborated by the range of values found in the magnetic measurements, particularly in Fig. 12, 13, and

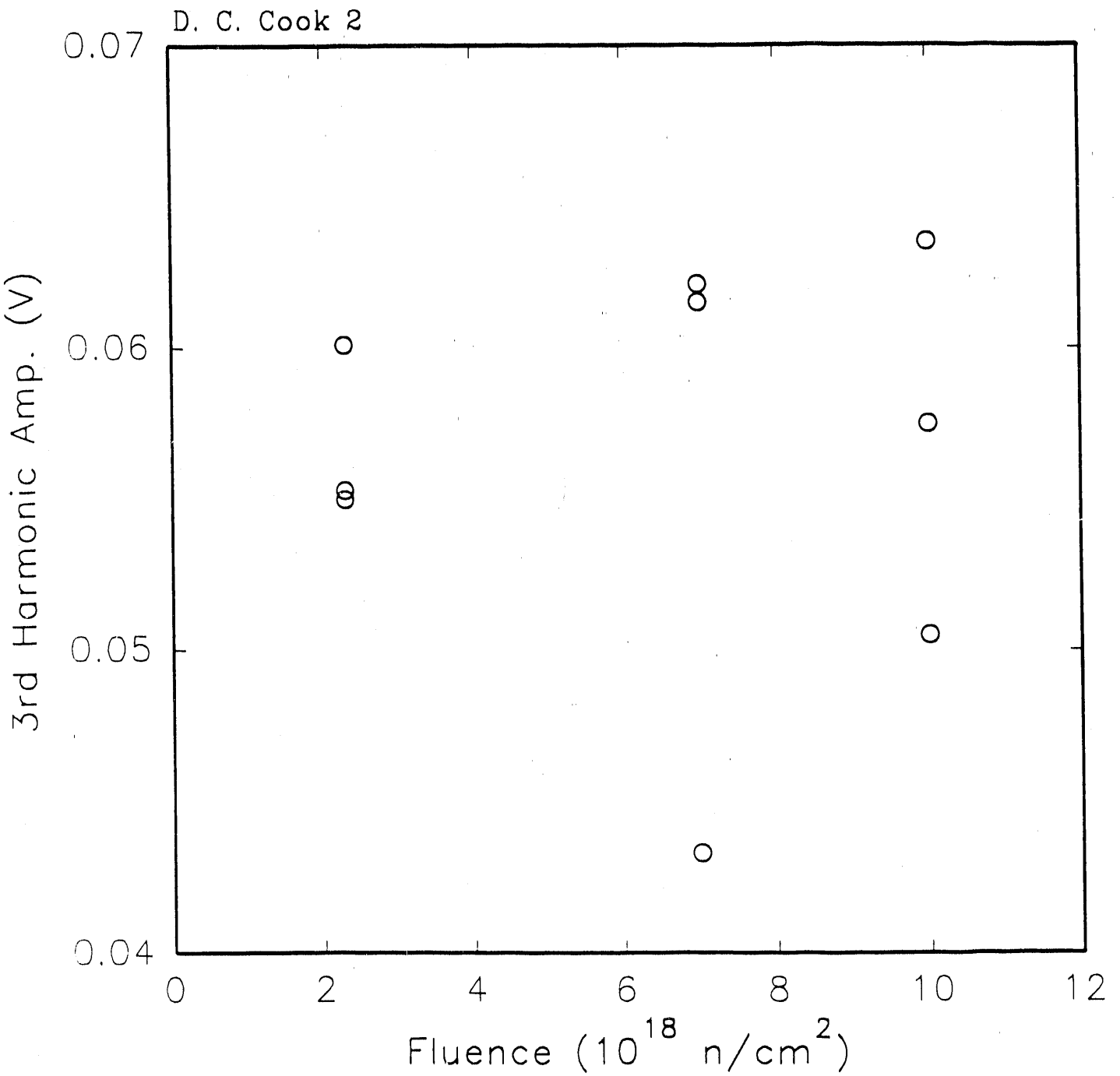

Fig. 12. Scatter plot for third harmonic signal amplitude (H_{max} level 2) vs. neutron fluence for D.C. Cook 2 reactor.

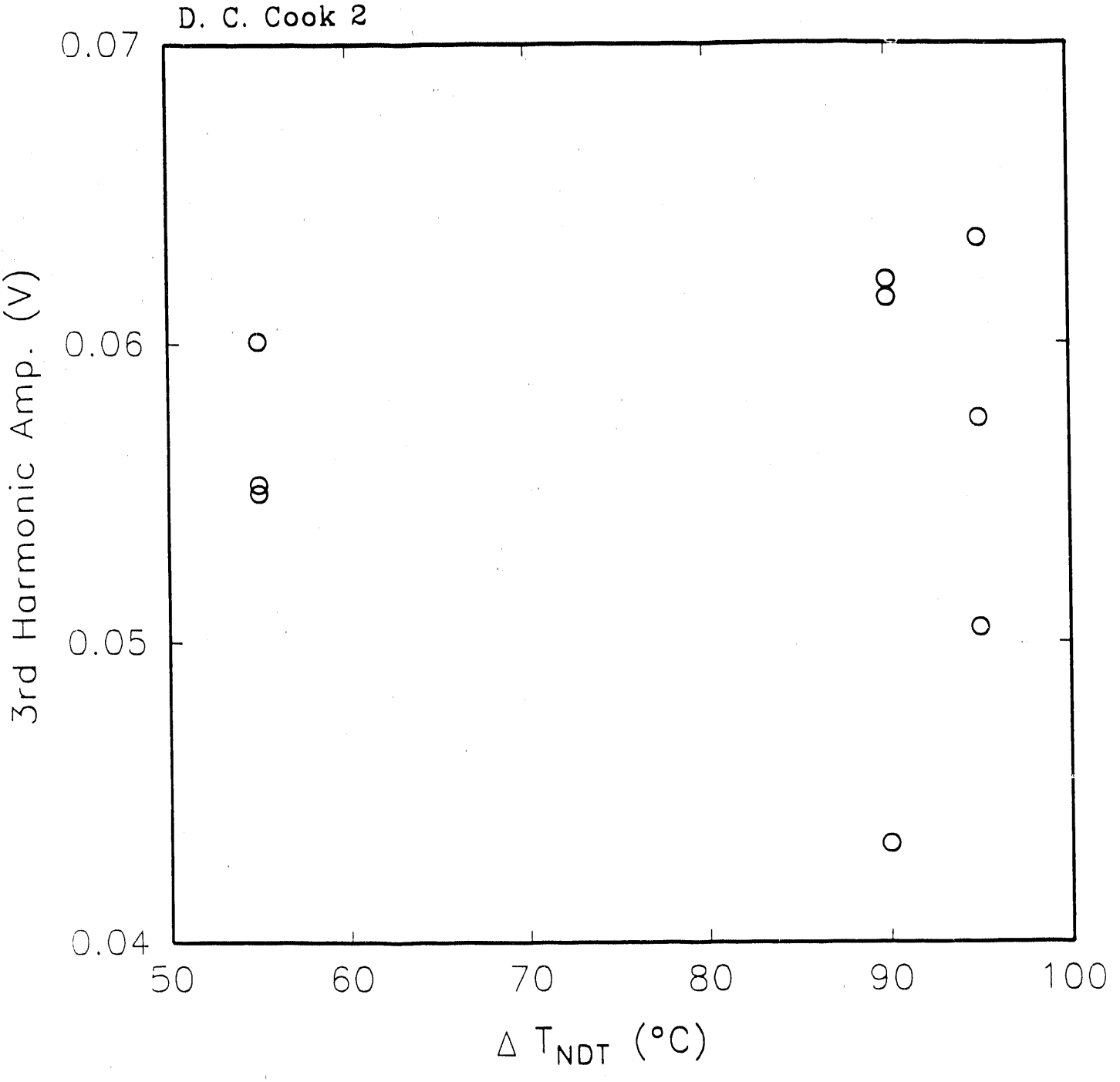

Fig. 13. Scatter plot for third harmonic signal amplitude (H_{max} level 2) vs. ΔT_{NDT} for D.C. Cook 2 reactor.

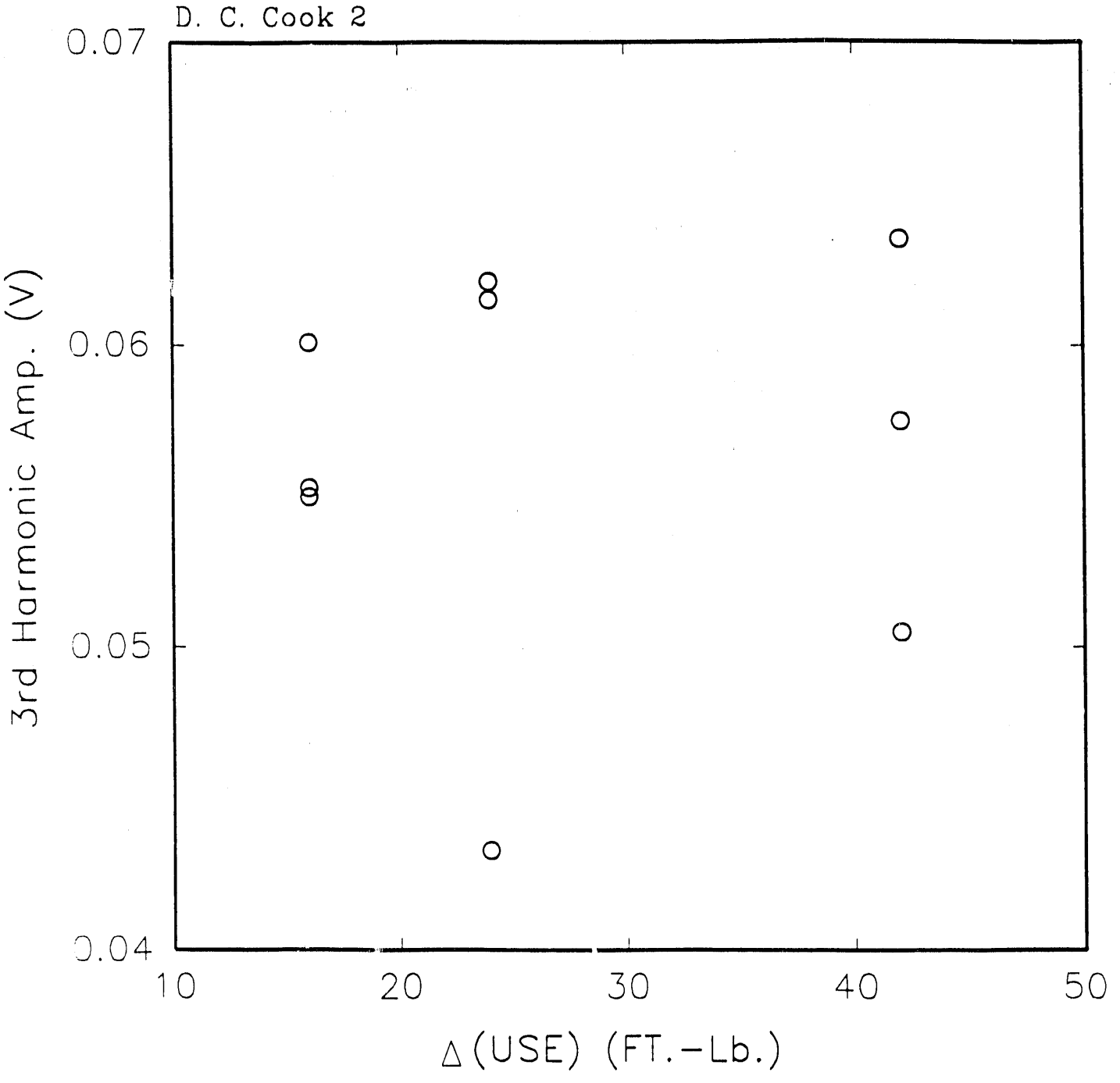

Fig. 14. Scatter plot for third harmonic signal amplitude (H_{max} level 2) vs. Δ(USE) for D.C. Cook 2 reactor.

14, for groups of samples that are supposed to have the same ΔT_{NDT} or Δ(USE).

Another important difference between the two reactor sites is that a low leakage core configuration was installed at the D.C. Cook 2 site between the second and third capsule samplings. Since the low leakage core configuration screens out the higher energy neutrons, a given neutron fluence does not necessarily correspond to the same amount of neutron damage, thus causing the leveling off in embrittlement seen in the third sample set L at the D.C. Cook site. The third sample set should therefore not correlate properly with the first and second sample set, thus offering a possible explanation for the very poor correlation found in the D.C. Cook 2 specimens. This however should more likely account for poor correlation with fluence, but not necessarily with embrittlement parameters.

On a more positive note, we return to the very good correlation found for the Indian Point 2 specimens. This suggests indeed that magnetic property measurement may be a potential way to monitor embrittlement in situ during down cycles or even possibly on an automated basis while the reactor is running.

The data so far suggests that techniques such as Barkhausen noise (BN) measurement or nonlinear harmonics (NLH) seem to offer the most potential for use in embrittlement monitoring. The physical theory is obviously challenged to explain why BN or NLH are better techniques for monitoring embrittlement than hysteresis loop properties such as coercivity, remanence, or permeability at the coercive point. One possibility for a purely experimental explanation is that the hysteresis loop properties were determined from only one digitized loop, whereas the Barkhausen and nonlinear harmonic amplitudes represent averages over more than one loop.

IV. FUTURE EXPERIMENTAL PLANS

A. Plans for additional study of magnetic NDE techniques for neutron embrittlement monitoring

There are two proposed techniques which have yet to be employed in our studies - magabsorption and MIVC. Both techniques require redesign of existing configurations in order to accommodate the small sample size. This redesign has been started and should be completed in two or three months.

Meanwhile, experimental measurements for the three techniques used so far will be expanded in order to possibly answer the several questions that have so far arisen. Among the possible paths that we shall take are the following:

1) A search will be made among our stored specimens to see if three sets of Charpy specimens exist for another reactor that either didn't have a low leakage core configuration during the time the samples were exposed or did have a low leakage core configuration at the time of all three samplings. The latter case is not probable since low leakage core configurations have been in use for a very short time. There may be other reactors besides Indian Point 2 which are old enough to have had at least three capsules pulled before modification to a low leakage core configuration. If we don't have three Charpy sets, it might be possible to obtain a third set if we have two already in our possession. If three Charpy sets can be found for another reactor, hysteresis loop, BN, and NLH measurements will be performed on such samples.

2) A test will be performed to see if digitizing 4 hysteresis loops and averaging the parameters obtained from them improves the correlation between hysteresis loop parameters and fluence and/or embrittlement parameters.

3) Instead of using 3 specimens per each fluence, 5 specimens per fluence will be tried, at least for the Indian Point 2 reactor in order to see if more specimens improve or diminish the correlation found so far.

4) The nonlinear harmonic data was taken at 1 Hz, which is quasi dc data. We will check to see if the excellent correlation for Indian Point 2 specimen remains when two other higher frequencies are chosen.

B. Plans for Second Year

In the second year, it was proposed that the magnetic NDE techniques be applied to the problem of biaxial stress measurements.

In the original proposal, a biaxial stress rig was to be built using a cruciform-shaped (viz. cross-shaped) specimen that could be stretched (or compressed) along two mutually perpendicular axes. Since then, structural engineers have suggested to us that only the central region of the cruciform specimen would be under true biaxial stress and that in order to do the study without a large amount of experimental error, the cruciform specimens (and accompanying rig) would have to be much larger than we proposed, which would be much more expensive.

On the other hand, it turns out that an alternative approach is available to us. From another project we have inherited a rig which allows one to pressurize a pipe (which creates positive hoop stress) and allows one to put tension or compression on the ends of the pipe. This arrangement creates a true biaxial stress condition along the pipe, except very near the ends of the pipe, thus providing a large area of uniform stress field. The pipe will have longitudinal (i.e. axial) compressive or tensile stress and tensile circumferential (i.e. hoop) stress. This will allow us to study biaxial stress in the situation of immediate energy interest - i.e. in piping itself. At the same time the new procedure will restrict experimental error and keep the experiment from being more costly than was proposed originally.

It is thus planned that we use the above pipe sample and loading arrangement in applying the five magnetic NDE techniques to the study of biaxial stress. The plan will be to find a procedure which allow the determination of both axial and hoop stress separately under stress conditions as close to the yield point as possible. Thus, the intent is to be able to inspect piping under high stress conditions and be able to make a quantitative statement about how much hoop and how much axial stress exists in the piping. It is expected that modeling will give guidance as to what procedure might be used for such a determination.

C. Plans for the Third Year

The third year will be one in which experimental and theoretical results will be consolidated and coordinated so as to design the best procedures for determining (1) neutron embrittlement and (2) biaxial stress.

During this time, procedures and theoretical predictions will be checked experimentally in a sequence of steps and stages in order to be able to suggest, at the end of the project, well-tested procedures for determining neutron embrittlement and biaxial stress.

V. THEORETICAL RESULTS AND PLANS

Some work was performed on the basic magnetomechanical hysteresis model in order to make the expression derived for the magnetostriction consistent with the ΔE effect, which requires that the magnetostrain be zero at magnetic saturation so that applied mechanical stress produces only elastic strain at saturation. This work was also partly supported by another sponsor and was presented in a paper[41] at the International Conference on Magnetism in Edinburgh, Scotland. A copy of the paper may be found in Appendix 2.

Also, importantly, work has been performed on another project to determine the dependence of magnetic properties on the angle between stress axis and magnetic field direction in cases of noncollinear stress and field. These new results will be used in making predictions about the effects of stresses along two perpendicular axes with magnetic field in yet a third direction. Thus the application of these angle-dependent magnetic property predictions in the second year to the case of biaxial stress is expected to be reaonsably straightforward because of these new results. This will offer an opportunity to consider the more difficult problem of stresses near the yield point and how magnetomechanical hysteresis modeling can be used to treat magnetic effects associated with stresses near or possibly even beyond the yield point, which is what would be of most interest in the case of pipeline.

Application of magnetomechanical hysteresis modeling to the problem of magnetic effects due to neutron embrittlement has been delayed until some experimental data has become available. This was done because it was felt that the experimental data would offer some guidance as to what needed explanation and some guidance as to what types of problems needed to be resolved with the help of modeling.

It is clear from the experimental results obtained so far that the best magnetic NDE techniques for monitoring neutron embrittlement so far seem to be dynamic techniques such as Barkhausen noise and nonlinear harmonics. These techniques involve the transform of time-dependent phenomena into frequency space out of which measurements are taken. At the moment, it is not clear why such measurements would be better indicators of embrittlement than static properties such as coercivity, remanence or permeability at the coercive point. Thus, an important problem would be to resolve this question.

It was proposed originally that magnetomechanical hysteresis modeling be applied to Barkhausen noise under this project. A preliminary treatment of that problem was discussed by M. Sablik and H. Kwun in a paper published earlier this year.[42] Jiles had noted that most Barkhausen activity occurs close to the coercive field,[10] suggesting that Barkhausen noise peaks at applied field H coinciding with the peak in the permeability. Bozorth[43] however presents data where the two peaks very clearly do not coincide. The application from the magnetomechanical hysteresis model is that the Barkhausen noise peak should correspond with the peak in the irreversible contribution to the permeability, not the peak in the permeability itself. In the magnetomechanical hysteresis model, it is possible to obtain the irreversible permeability and find its peak as a function of H. The peak position of the irreversible permeability was located at higher H than the peak in the permeability itself, just as shown by the data in Bozorth.[43] This result was fine, but as pointed out by Bertotti[44] it did not give an expression for Barkhausen noise itself.

What will be needed for the questions that confront us concerning neutron embrittlement is a complete derivation and expression for Barkhausen noise amplitudes. Two features will have to be explicit in the expression - (1) dependence on permeability, so that Barkhausen noise will peak near the peak in permeability and (2) proportionality to some power of the domain wall pinning site density, since

the Barkhausen amplitude will be greater when more domain walls are unpinned per unit field.

Alessandro et al[45,46] develop an expression for the Barkhausen noise power spectrum as

$$F_{BN}(\omega) = 4S\dot{M}\frac{A}{(\sigma G)^2}\frac{\omega^2}{(\omega^2 + \tau^{-2})(\omega^2 + \tau_c^{-2})}, \qquad (1)$$

Here $\dot{M}$ is the rate of change of magnetization with time near the coercive point, (where $\dot{M} = \mu\dot{H}$), μ is the permeability, S is an average domain wall surface area, σ is the electrical conductivity, G = 0.1356, A is an undefined constant, $\tau=\sigma GS\mu$, $\tau_c = \xi/S\dot{M}$, ξ is a magnetic correlation length, and ω is angular frequency. This expression has the general requirements of proportionality to permeability but folded into a more complex dependence on permeability so that the peak in BN does not occur at the same H as permeability. In addition, dependence on σ^{-2} is equivalent to dependence on ρ^2, where ρ is the electrical resistivity. The resistivity ought to depend at least in part on pinning site density though its impurity or defect scattering contribution to the resistivity. So, potentially, the expression in eq. (1) might indeed be usable for interpreting Barkhausen noise data. The expression might need to be averaged over a hysteresis loop with the hysteretic expression for permeability substituted for μ instead of permeability at the coercive point. Some approximations however were made in deriving the expression in eq. (1), and its is felt that the theory for a Barkhausen noise expression may need additional attention.

An alternative expression for Barkhausen noise is given by J. Kameda and R. Ranjan[47]

as

$$V_{BN}^{MAX} = \gamma\{\beta_n \frac{dN_n}{dH} + \frac{L}{\delta}\frac{dN_g}{dH} + \left(\frac{N_g}{\delta}\right)\frac{dL}{dH}\} A\frac{dH}{dt} \qquad (2)$$

where V_{BN}^{MAX} refers to the maximum voltage associated with the Barkhausen burst, γ is a numerical coefficient related to the atomic magnetic moment, β_n is the coefficient related to the spike shape of nucleated domains, N_n is the density of nucleated domain walls, N_g is the density of jumping domain walls, L is the average displacement of growing domains, δ is the domain wall thickness, and A is the effective surface skin area, which varies with dH/dt because of eddy current loss. Further study will be needed to see if eq. (2) can be related to eq. (1) and to see whether part of what multiplies dH/dt in eq. (2) can be represented as permeability and pinning site density.

In the coming months, an effort will be made to relate all of these equations to the macroscopic magnetomechnical hysteresis model and so obtain a result for Barkhausen noise that relates the microscopic mechanism and macroscopic modeling.

In addition, the nonlinear harmonics results will be studied theoretically using our previous techniques for treating 1Hz harmonics,[4] but relating the results to a more microscopic interpretation so that embrittlement effects could be understood. Since the nonlinear harmonics will also be studied at higher frequencies, magnetic relaxation effects[48-51] and eddy current losses[52-56] will also be added to the theoretical development in the second year.

Finally, the MIVC measurement technique and magabsorption technique will be studied

in such a way as to relate the detected results to microstructural effects connected with embrittlement. As part of the development, the eq. of motion technique, used to solve for MIVC results at high fields,[57,58] will be extended to low fields taking polycrystallinity into account, as proposed in our original proposal. Thus, field-dependent velocity changes seen at low field for the two shear wave polarizations[20,21] and for longitudinal waves[22] will be derivable. Work is already starting on this development, but is not expected to be completed until the second year. The original hysteretic magnetomechanical model for magabsorption[6,7] will also be expanded so that microstructural effects from neutron embrittlement can be considered.

In the second year, as mentioned earlier, work done elsewhere on noncollinear stress and field will be applied to the problem of biaxial stress. Also, in the second year, magnetic effects due to stresses near the yield point and beyond will be considered.

In the third year, consolidation will occur between experiment and theory. Theoretical results will be tested experimentally. The theory will also be used to suggest procedures that will most advantageously use the magnetic NDE techniques, particularly in the case of biaxial stress. These procedures will be tested. In the meantime final adjustments will be made in the modeling, and whatever problems are still outstanding will be addressed.

REFERENCES

1. L.E. Steele, "Newtron Irradiation Embrittlement of Reactor Pressure Vessel Steels," Nuclear Safety 17, 327 (1976).

2. G.L. Burkhardt, H. Kwun, A.E. Crouch, and D.A. DesNoyer, "Review of Stress Measurement Techniques for Pipelines," in Damage Assessment, Reliability, and Life Prediction of Power Plant Components, ed. R.N. Pangborn (ASME, 1990), PVP, Vol. 193/NDE, Vol. 8, from Proc. Pressure Vessels and Piping Conference, Nashville TN (June 1990), pp. 95-103.

3. M.J. Sablik, H. Kwun, G.L. Burkhardt, and D.C. Jiles, "A Model for the Effect of Tensile and Compressive Stress on Ferromagnetic Hysteresis," J. Appl. Phys. 61, 3799 (1987).

4. M.J. Sablik, G.L. Burkhardt, H. Kwun, and D.C. Jiles, "A Model for the Effect of Stress on the Low-Frequency Harmonic Content of the Magnetic Induction in Ferromagnetic Materials," J. Appl. Phys. 63, 3930 (1988).

5. M.J. Sablik and D.C. Jiles, "A Model for Magnetostriction Hysteresis," J. Appl. Phys. 64, 5402 (1988).

6. M.J. Sablik, W.L. Rollwitz, and D.C. Jiles, "A Model for Magabsorption as an NDE Tool for Stress Measurement," in Proc. 17th Symposium on NDE, San Antonio TX, Apr 17-20, 1989, ed. F.A. Iddings (NTIAC, Southwest Research Institute, San Antonio TX 1989), p. 212-223.

7. M.J. Sablik, "Modeling Stress Dependence of Magnetic Properties for NDE of Steels," Nondestructive Testing and Evaluation 5, 49 (1989).

8. H. Kwun and G.L. Burkhardt, "Electromagnetic Techniques for Residual Stress Measurements," in Metals Handbook Vol. 17, Nondestructive Evaluation and Quality Control, ed. S.R. Lampman and T.B. Zorc (ASM International, 1989) pp. 159-163.

9. W.L. Rollwitz, "Magabsorption NDE," in Metals Handbook, Vol. 17, Nondestructive Evaluation and Control, ed. S.R. Lampman and T.B. Zorc (ASM International, 1989), pp. 143-158.

10. D.C. Jiles, "Review of Magnetic Methods for Nondestructive Evaluation," NDT International 21, 311 (1988).

11. H. Kwun and G.L. Burkhardt, "Effects of Grain Size, Hardness, and Stress on the Magnetic Hysteresis Loops of Ferromagnetic Steels," J. Appl. Phys. 61, 1576 (1987).

12. H. Kwun and G.L. Burkhardt, "Effects of Stress on the Harmonic Content of Magnetic Industion in Ferromagnetic Material," Proc. 2nd Natl. Seminar on NDE of Ferromagnetic Materials, Houston TX (March 1986), available from Dresser Industries, Houston TX.

13. H. Kwun and G.L. Burkhardt, "Nondestructive Measurement of Stress in Ferromagnetic Steels Using Harmonic Analysis of Induced Voltage," NDT International 20, 167 (1987).

14. G.L. Burkhardt and H. Kwun, "Application of the Nonlinear Harmonics Method to Continuous Measurement of Stress in Railroad Rail," in Proc. of the 1987 Review of Progress in

Quantitative NDE, Vol. 7B, ed. D.O. Thompson and D.E. Chimenti (Plenum Press, 1988), p. 1413.

15. R.L. Pasley, "Barkhausen Effect -- An Indication of Stress," Mater. Eval. 28, 157 (1970).

16. J.C. McClure, Jr., and K. Schroder, "The Magnetic Barkhausen Effect," CRC Crit. Rev. Solid State Sci. 6, 45 (1976).

17. G.A. Matzkanin, R.E. Beissner, and C.M. Teller, "The Barkhausen Effect and Its Applications to Nondestructive Evaluation," State of the Art Report, NTIAC-79-2, Nondestructive Testing Information Analysis Center, Southwest Research Institute (1979).

18. H. Kwun, "Investigation of the Dependence of Barkhausen Noise on Stress and the Angle Between the Stress and Magnetization Directions," J. Magn. Magn. Mater. 49, 235 (1985).

19. G.L. Burkhardt and H. Kwun, "Measurement of Residual Stress Around a Circular Patch Weld Using Barkhausen Noise," in Rev. Progr. in Quantitative NDE, ed. D.O. Thompson and D.E. Chimenti (Plenum, NY, 1989), Vol 8A, pp. 1053-1060.

20. H. Kwun and C.M. Teller, "Tensile Stress Dependence of Magnetically Induced Ultrasonic Shear Wave Velocity Change in Polycrystalline A-36 Steel," Appl. Phys. Lett. 41, 144 (1982).

21. H. Kwun and C.M. Teller, "Stress Dependence of Magnetically Induced Velocity Change in Polycrystalline A-36 Steel," J. Appl. Phys. 54, 4856 (1983).

22. H. Kwun, "Effects of Stress on Magnetically Induced Velocity Changes for Ultrasonic Longitudinal Waves in Steels," J. Appl. Phys. 57, 1555 (1985).

23. H. Kwun, "A Nondestructive Measurement of Residual Bulk Stresses in Welded Steel Specimens by Use of Magnetically Induced Velocity Changes for Ultrasonic Waves," Mater. Eval. 44, 1560 (1986).

24. H. Kwun, "Measurement of Stress in Steels Using Magnetically Induced Velocity Changes for Ultrasonic Waves," in Nondestructive Characterization of Materials II, ed. J.F. Bussiere, J.R. Monchalin, C.O. Ruud, and R.E. Green, Jr. (Plenum Press, 1987), p. 633.

25. M. Namkung and D. Utrata, "Nondestructive Residual Stress Measurements in Railroad Wheels Using the Low-Field Magnetoacoustic Test Method", in Proc. 1987 Review of Progress in Quant. NDE, ed. D.O. Thompson and D.E. Climenti (Plenum Press, 1988), p. 1429.

26. D.J. Buttle, G.A.D. Briggs, J.P. Jakubovics, E.A. Little, and C.B. Scruby, "Magnetoacoustic and Barkhausen Emission in Ferromagnetic Materials," Phil. Trans. Roy. Soc. London A320, 363 (1986).

27. D.J. Buttle, E.A. Little, C.B. Scruby, G.A.D. Briggs, and J.P. Jakubovics, "A Study of Neutron Irratiation Damage in α-Iron with Magnetoacoustic and Barkhausen Emission," Proc. Roy. Soc. London A414, 221 (1987).

28. E.A. Little, D.J. Buttle, and C.B. Scruby, "Radiation Damage Studies in Model Ferritic Alloys

Using Micromagnetic Techniques," Phys. Stat. Sol. (a) 112, 55 (1989).

29. J.R. Barton and R.D. Wylie, "Development of Nondestructive Testing Instrumentation for Reactor Pressure Vessels," Sixth Quarterly Report, Contract No. AT(11-1)-1243, prepared for Joint US/Euratom Research and Development Program (July 1964).

30. M.S. Wechsler and R.G. Berggren, "Radiation Embrittlement of Reactor Pressure Vessels," Nuclear Safety 4, 42 (1962).

31. D.G. Cadena, Jr., "Neutron Embrittlement of Steels in Nuclear Pressure Vessels," Nondestr. Test. Eval. 6, 95 (1991).

32. A. Zentko, M. Timko, and P. Duhaj, "Effect of Neutron Irradiation on the Magnetic Properties of Amorphous $Fe_{47}Ni_{25}B_{18}Si_{10}$ Alloys," Phys. Stat. Sol. (a) 66, K125 (1981).

33. R.D. Brown, J.R. Cost, and J.T. Stanley, "Irradiation-Induced Decay of Magnetic Permeability of Metglas 26055-3 and Mumetal," J. Nucl. Mater. 131, 37 (1985).

34. H. Soffel, "The Effect of Radiation with Fast Neutrons on the Saturation Remanence of a Basalt," Z. fur Geophysik 37, 519 (1971).

35. D.J. Buttle, Harwell Research Laboratory, private communication.

36. K. Masubari, Analysis of Welded Structures (Pergamon Press, NY, 1980), pp. 350-3.

37. H. Kayano, M. Narui, S. Ohta, and S. Morozumi, "Irradiation Embrittlement of Neutron-Irradiated Ferritic Steel," J. Nucl. Mater. 133& 134, 649 (1985).

38. K. Suzuki, "Neutron Irradiation Embrittlement of ASME SA508, C1.3 Steel," J. Nucl. Mater. 108& 109, 443 (1982).

39. L.E. Steele, "Radiation Embrittlement of Reactor Pressure Vessels," Nucl. Eng. Des. 3, 287 (1966).

40. ENDF/B-IV, Dosimetry Tape 412, Mat. No. 6417 (26-Fe-54), July 1974, and L.E. Steele and C.Z. Serpan, Jr., "Analysis of Reactor Pressure Vessel Effects Surveillance Programs," ASTM STP 481, Dec. 1970.

41. M.J. Sablik and S.W. Rubin, "Relationship of Magnetostrictive Hysteresis to the ΔE Effect," presented at the International Conference on Magnetism, Edinburgh, Scotland, Sept. 1991 and to be published in J. Magn. Magn. Mater.

42. M.J. Sablik and H. Kwun, "Hysteretic Model for Barkhausen Noise and the Magnetically Induced Velocity Change of Ultrasonic Waves in Ferromagnets Under Stress," J. Appl. Phys. 69, 5791 (1991).

43. R.M. Bozorth, Ferromagnetism (Van Nostrand, NY, 1951), p. 529.

44. G. Bertotti, private communication.

45. B. Alessandro, C. Beatrice, G. Bertotti, and A. Montorsi, "Domain Wall Dynamics and Barkhausen Effect in Metallic Ferromagnetic Materials. I. Theory," J. Appl. Phys. 68, 2901 (1990).

46. B. Alessandro, C. Beatrice, G. Bertotti, and A. Montorsi, "Domain Wall Dynamics and Barkhausen Effect in Metallic Ferromagnetic Materials. II. Experiments," J. Appl. Phys. 68, 2908 (1990).

47. J. Kameda and R. Ranjan, "Nondestructive Evaluation of Steels Using Acoustic and Magnetic Barkhausen Signals -- I. Effect of Carbide Precipitation and Hardness," Acta Metall. 35, 1515 (1987).

48. M. Guyot, T. Merceron, and V. Cagan, "Domain Wall Dynamics and Relexation Through the Frequency Dependence of Hysteresis Loops, " J. Appl. Phys. 57, 4180 (1985).

49. G. Gremaud, "The Hysteretic Damping Mechanisms Related to Dislocation Motion," J de Physique 48, Colloque C8, Supp. 12, p. C8-15 (1987).

50. Y. Nakatani, Y. Uesaka, and N. Hayashi, "Direct Solution of the Landau-Lifschitz Gilbert Equation for Micromagnetics," Jap. J. Appl. Phys. 28, 2485 (1989).

51. T. Plefka, "Nonlinear Damping in Spin Systems: Ferromagnetic Infinite Range Exchange Interactions," Physica A162, 477 (1990).

52. D. Carpenter and R.J. Hill, "The Effects of Magnetic Saturation, Hysteresis, and Eddy Currents on Rail Track Impedance," Proc. 1989 Joint ASME/IEEE Railroad Conference, Philadelphia PA, p. 73.

53. G. Bertotti, F. Fiorillo, P. Mazzetti, and G.P. Soardo, "Dynamics of Microscopic Magnetization Processes and Magnetic Losses," J. Appl. Phys. 53, 8287 (1982).

54. G. Bertotti, "Physical Interpretation of Eddy Current Losses in Ferromagnetic Materials. I. Theoretical Considerations," J. Appl. Phys. 57, 2110 (1985).

55. G. Bertotti, "Physical Interpretation of Eddy Current Losses in Ferromagnetic Materials. II. Analysis of Experimental Results," J. Appl. Phys. 57, 2118 (1985).

56. H.T. Savage and M.L. Spano, "Theory and Application of Highly Magnetoelastic Metglas 2605SC," J. Appl. Phys. 53, 8082 (1982).

57. J.R. Cullen, S. Rinaldi, and G.V. Blessing, "Elastic Properties of Magnetostrictive Rare Earth Iron Alloys," Proc. Rare Earth and Actinides Conference, Durham, England, 1977, in Inst. Phys. Conf. Series No. 37 (IOP, London, 1978), p. 79.

58. S. Rinaldi and J. Cullen, "Resonant Coupling of Shear Waves in Magnetostrictive Rare Earth-Iron Compounds," Phys. Rev. B18, 3677 (1978).

59. H. Kwun, G.L. Burkhardt, and C.M. Teller, "Ultrasonic Transducers Performance Requirements, Phase II," Final Report, SwRI Project No. 15-5468, NTIS Accession No. ADA 101169 (June, 1981).

APPENDIX 1

Linear Correlation Coefficient

Appendix 1

Linear Correlation Coefficient

Consider n number of samples for the two parameters X and Y which are $(X_1, Y_1), (X_2, Y_2), \ldots,$ and (X_n, Y_n). The linear correlation coefficient R between the two parameters is defined by

$$R = \frac{\Sigma_i \, x_i \, y_i}{(\Sigma_i \, x_i^{\,2} \Sigma_i \, y_i^{\,2})^{1/2}} \qquad (1)$$

where Σ_i is the summation over $i = 1$ to n, and x_i and y_i represent the deviations of the ith sample (X_i, Y_i) from the sample mean of the two parameters $(\overline{X}, \overline{Y})$, i.e.

$$x_i = X_i - \overline{X}, \; where \; \overline{X} = \frac{\Sigma_i \, X_i}{n} \;, \; and$$

$$y_i = Y_i - \overline{Y}, \; where \; \overline{Y} = \frac{\Sigma_i \, Y_i}{n} \;. \qquad (2)$$

The linear correlation coefficient R varies between -1 and +1, depending on the closeness of the relationship between the samples. Positive values of R indicate a tendency to have a linear relationship with positive slope. Conversely, negative values of R indicate a tendency to have a linear relationship with a negative slope. When $|R| = 1$, the two parameters are said to be perfectly related. In this case, any change in one parameter is always accompanied by a proportional change in the other. When $R = 0$, two parameters are said to be unrelated. In this case, two parameters vary randomly.

Figure A1 shows examples of scatter diagrams of two parameters with a range of linear correlation coefficients. It can be seen that the higher $|R|$, the smaller the degree of scatter from the lines drawn in the figure. The two lines in each diagram represent a least square fit of the linear relationship between the two parameters. One of the lines (indicated by A) is obtained by assuming the parameter on the Y axis is dependent on the parameter on the X axis, and the other line (indicated by B) by assuming the parameter on the X axis is dependent on the parameter on the Y axis.

Equation (1) can be rewritten as:

$$R = \left[\frac{\left(\Sigma_i \, x_i \, y_i\right)^2}{\left(\Sigma_i \, x_i^{\,2} \Sigma_i \, y_i^{\,2}\right)} \right]^{1/2}$$

$$= \left[\left(\frac{\Sigma_i \, x_i \, y_i}{\Sigma_i \, x_i^{\,2}} \right) \left(\frac{\Sigma_i \, x_i \, y_i}{\Sigma_i \, y_i^{\,2}} \right) \right]^{1/2}$$

$$= \left(b_{xy} \, b_{yx}\right)^{1/2}$$

where $b_{xy} = \dfrac{\Sigma_i \, x_i \, y_i}{\Sigma_i \, y_i^{\,2}}$ *and*

$$b_{xy} = \frac{\Sigma_i \, x_i \, y_i}{\Sigma_i \, x_i^{\,2}}. \qquad (3)$$

Note that b_{xy} is the slope of the least square fitted line obtained by assuming parameter X is a function of parameter Y. Similarly, b_{xy} is the slope of the least square fitted line obtained by assuming parameter Y is a function of parameter X. In statistics, this slope is usually called the linear regression coefficient. Therefore, equation (3) states that the correlation coefficient, R, is the geometric mean of the slope of the two least square fitted lines.

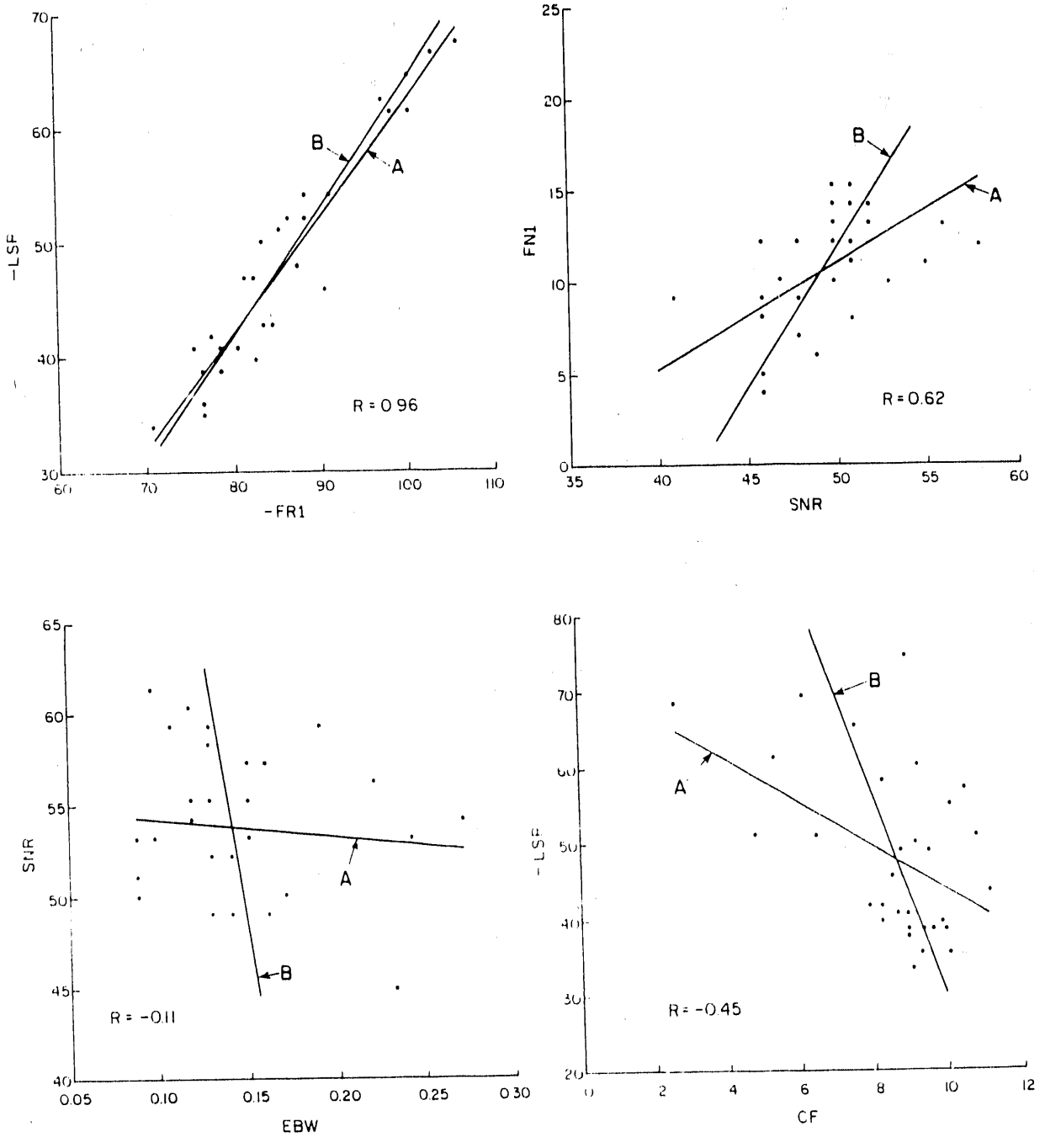

Fig. A1 Examples of scatter plots for data having various R values. R is the linear correlation coefficient. A represents the least square fit line obtained by assuming the parameter of the Y axis is dependent on the parameter of the X axis. B represents the least square fit line obtained by assuming the parameter of the X axis is dependent on the parameter of the Y axis. (Ref. 59).

APPENDIX 2

Paper, "Relationship of Magnetostrictive Hysteresis to the ΔE Effect", M. Sablik and S.W. Rubin

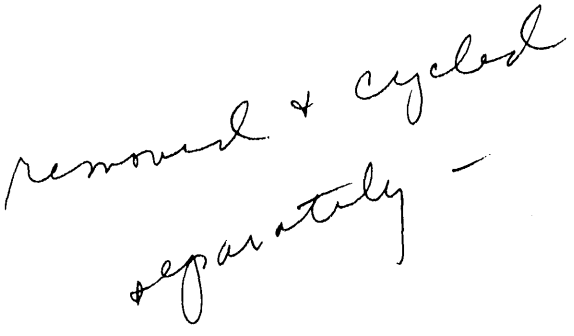

APPENDIX 3

Professional Data Sheets on Co-Investigators

MARTIN J. SABLIK
Staff Scientist
Department of Space Sciences
Instrumentation and Space Research Division

B.A. in Physics, Cornell University, 1960
M.S. in Physics, University of Kentucky, 1965
Ph.D. in Physics, Fordham University, 1972

With over 25 years of professional experience, Dr. Sablik is primarily a theoretical physicist with broad experience in pure and applied physics.

In the field of condensed matter, Dr. Sablik has principally focussed on the theory of magnetic properties of materials. He has developed models to explain the effect of uniaxial stress on magnetic hysteresis, magnetostriction hysteresis and other magnetic and magnetoelastic properties in steels, rare earth intermetallics and amorphous metallic glasses. He has published fundamental work on the theory of quadrupolar excitations in rare earth compounds and on the theory of the aspherical coulomb scattering contribution to the electrical resistivity. He has used Monte Carlo computer simulation to study magnetic phase transitions. His doctoral research treated the theory of nuclear spin-lattice relaxation rates and of the spin wave stiffness constant in dilute transition metal alloys. Recently, he has been doing research on high temperature superconductivity, both theoretical and experimental.

Since joining Southwest Research Institute in 1980, Dr. Sablik has also specialized in computational physics and large-scale computer modeling of physical systems. He has participated in structural vibration studies, employing both the finite element and statistical energy analysis techniques, and has produced papers on vibration transmission in beam networks. He has utilized coupled circuit theory to develop a computer model for finding eddy currents induced in metallic materials. He has participated in physical modeling for various electromagnetic nondestructive evaluation techniques and has coauthored several papers in this area. Most recently, he has published a number of papers on computer simulations of various electrostatic analyzers used for studying charged particle distributions in space environments. Dr. Sablik has the ability to combine his knowledge of physics and mathematics with computer modeling and is able to treat many diverse problems.

Prior to joining the staff at Southwest Research Institute, Dr. Sablik taught physics and computer science at both the graduate and undergraduate levels at Fairleigh Dickinson University, where he also involved students in his research.

In his early pre-doctoral career he participated in experimental solid state research involving $BaTiO_3$, other ferroelectrics, wide gap semiconductors, alkaline earth oxides, asbestos materials, maser materials, and organic and inorganic electroluminescent phosphors. He also specialized in crystal-growing techniques in his work at Martin Marietta.

PROFESSIONAL CHRONOLOGY: Summer technical positions (Sprague Electric Company, 1959; Johns-Manville Corporation, 1960; Dow Chemical Company, 1961); junior engineer, Martin Marietta Corporation, 1962-3; half-time instructor, University of Kentucky, 1963-5; Fairleigh Dickinson University (research associate, 1965-7; instructor, 1967-9, Rutherford Campus; on-leave, NSF graduate trainee, 1969-71; instructor, Teaneck Campus, 1971-2; NSF summer post-doctoral fellow, 1972-3; assistant professor of physics, 1972-6; associate professor of physics, 1976-80); Southwest Research Institute, 1980-(consultant; senior research physicist, instrumentation and space research division, 1980-7, staff scientist, 1987-).

Memberships: American Physical Society, Institute of Electrical and Electronics Engineers, American Association of Physics Teachers, American Society of Nondestructive Testing, American Geophysical Union.

July/89

HEGEON KWUN, Ph.D.
Senior Research Scientist
Department of Nondestructive Evaluation Science and Research

B.S. in Applied Physics, Seoul National University, 1970
M.S. in Physics, Brown University, 1976
Ph.D. in Physics, Brown University, 1980

Dr. Kwun is an experimental physicist with experience in the fields of nondestructive evaluation (NDE), magnetics, nonlinear effects, solid state physics, and low-temperature physics.

Since coming to Southwest Research Institute in 1980, Dr. Kwun has been engaged primarily in the application of ultrasonic and magnetics to special NDE problems. He has developed a patented nondestructive residual stress measurement method based on his research on the stress dependence of magnetically induced velocity changes (MIVC) for ultrasonic waves in ferromagnetic materials. The MIVC method has successfully been applied to measuring residual welding stresses, particularly bulk stresses, in samples of structural bridge steels. He has also been involved in the development of ultrasonic and electromagnetic sensors for NDE of material. In addition, he has recently developed a new method for NDE of wire or synthetic ropes called the transverse impulse-vibration method. This method, for which a patent is pending, can inspect a long rope over several hundred feet within a few seconds from a single location.

His current research activities and interests include NDE of composite materials, further development of NDE methods for wire or synthetic ropes, the effect of mechanical stress on the magnetic properties of ferromagnetic steels, development and application of techniques for characterizing magnetic materials, sensor development, and investigation of the properties of new high-temperature super-conducting ceramic materials. Dr. Kwun has authored 31 scientific papers which have been published in scientific journals and has been awarded two patents.

PROFESSIONAL CHRONOLOGY: Lieutenant, Republic of Korea Army, Signal corps, 1970-72; teaching assistant, Seoul National University, 1972-74; Brown University, 1974-80(teaching assistant, 1974-75; research assistant, 1975-79; research associate, Metals Research Laboratory, 1979-80; Southwest Research Institute, 1980-(research scientist, Instrumentation Research Division, 1980-83; senior research scientist, Instrumentation Research Division, 1983-85; senior research scientist, Department of Nondestructive Evaluation Science and Research, 1985-).

Memberships: American Physical Society and American Society for Nondestructive Testing.

DAVID G. CADENA, JR.
Radiation Safety Officer
Department of Energy Conversion and Combustion Technology

B.S. in Physics, St. Mary's University, 1957
M.S. in Physics, St. Mary's University, 1970

Mr. Cadena's background includes experience as a reactor physicist at the Savannah River Plant, particularly in startup and performance instrumentation. He has done basic research using electron spin resonance (ESR) to study the effects of ionizing radiation on biological materials and for the development of a tissue equivalent dosimeter system. His work experience includes eddy current inspection of nuclear power systems components and instrumentation development of photometric measuring systems with computerized data reduction techniques. He has worked on the field evaluation of a radon-radon daughter dosimetry system for underground uranium miners and is responsible for the radiological control of the opening and testing of reactor pressure vessel surveillance capsules.

Since 1968, he has served as health physicist with responsibility for training radiation workers and for the radiological safety of all SwRI personnel. He has assisted in the development of a computerized radiation exposure record-keeping system to keep track of SwRI transient worker exposures. He is currently serving as Radiation Safety Officer and Secretary of the Radiological Health and Safety Committee. This includes responsibility for industrial radiographic operations, control of all radioactive and contaminated equipment, radioactive material shipments, radioactive waste disposal, and operation of the high-level Cobalt 60 hot cells. He has served as an active member of the Atomic Industrial Forum subcommittee on Occupational Radiation exposure and the subcommittee on high-level waste. He has served as president of the South Texas Chapter of the Health Physics Society. His publication credits include papers on dosimetry systems, on effects of radiation on biological materials at cryogenic temperatures, and on ESR studies of biological systems.

PROFESSIONAL CHRONOLOGY:Technician (part-time), IBM operations, Lackland Air Force Base, 1956; technician (part-time), ESR instrumentation, Chemical Physics Section, Physics Department, Southwest Research Institute, 1956-7; reactor physicist, E.I. DuPont de Nemours and Company, Inc. (South Carolina), 1957-60; Southwest Research Institute, 1964-(assistant research physicist, Department of Physical and Biological Sciences, 1964-8; research physicist, Department of Physical and Biological Sciences, 1968-73; senior research physicist, Department of Vehicle and Traffic Safety, Automotive Research Division, 1973; radiation safety officer, Department of Vehicle and Traffic Safety, Automotive Research Division; 1974-81; radiation safety officer, Department of Energy Conversion and Combustion Technology, Fuels and Lubricants Research Division, 1981-).

Memberships: National Health Physics Society, Research Scientific Association (local chapter of Sigma Xi).

Rev Feb/87

WILLIAM L. ROLLWITZ
Institute Scientist
Radiofrequency Spectroscopy and Electronic Instrumentation
Instrumentation and Space Research Division
B.S. in E.E., Massachusetts Institute of Technology, 1950
M.S. in E.E., Massachusetts Institute of Technology, 1952
Graduate study in Physics, Trinity University, 1963-1967

With over 34 years in research and development, Mr. Rollwitz is experienced in all phases of Radiofrequency Resonance Absorption Spectroscopy (RRAS), which includes Nuclear Magnetic Resonance (NMR), Solid State NMR Imaging (STNMRI), Magnetic Resonance Imaging (MRI), Magnetic Resonance detection of cancer, Nuclear Quadrupole Resonance (NQR), Zero Field Nuclear Magnetic Resonance (ZFNMR), NMR/NQR Level-Crossing Measurements, Electronic Magnetic Resonancce (EMR,ESR, or EPR), and Microwave Molecular Absorption, as well as all phases of electronic instrumentation to perform physical measurements. Magnetic Resonance Imaging techniques have been used to develop a dedicated NMR device that is inexpensive enough to screen for breast cancer. This unit will be expanded to detect cancer in the urethra, prostate, colon, uterus, and cervix. Steady-State Nuclear Magnetic Resonance instruments have been developed to determine (1) the percentage of moisture in Processed foods, grains, and other hygroscopic materials in static samples and flowing process streams and (2) the amounts of hydrogen and aluminum in flowing solid propellant. A method has been developed using superconducting RF coils to increase the steady-state detection sensitivity by 100,000 times. Transient Nuclear Magnetic Resonance Instruments have been developed to determine (1) the moisture percentage, without weighing, in coal, explosives, starches, processed foods, and grains; (2) the binding states of moisture in living tissue and hygroscoping materials; (3) the presence of hidden illegal drugs; (4) the presence and identification of hidden explosives; (5) qualitative and quantitative analysis of explosives; (6)water and fat concentrations in living animals; amd (7) mass flow, flow velocity, calorific value, and proximate analysis of flowing coal. Magnetic Properties are being measured with the technique of Magnetoabsorption in materials, such as soils, rocks ferromagnetic metals, ferromagnetic coatings on nonferromagnetic metals and ferromagnetic powders. Magnetoabsorption equipment has been developed to measure the magnitude, direction, and type (compression or tension) of stress in ferromagnetic metals and nonferromagnetic metals with ferromagnetic coatings. Hidden Object Detectors have been developed that use (1) induction coils with ferrite cores, (2) magnetoabsorption signals from the soil to detect voids caused by nonmetallic mines, and (3) a combination of the induction and magnetoabsorption techniques to both detect and identify the composition of an object. Temperature has been measured with sensors using properties such as contact potential, magnetic permeability, and dielectric constant. The temperatures of the bearings and the pistons in an internal combustion engine have been telemetered using a capacitor as a sensor in a single-transistor oscillator and a power source driven by the motion of the piston. The system has a sensitivity of 1000 Hertz per °F over the range of 100°F to 600°F. Electron Magnetic Resonance was used to find the effects of microwave radiation on biological tissue (lens of the eye), the decay rates of the free electrons caused by gamma rays, and the free electron concentration in coals, which can be used to determine the carbon concentration and the calorific value. Electrostatic techniques have been used to collect and size aerosol particles. The above work has produced over 100 papers in the above field 15 patents have been issued and four patent applications are pending.

PROFESSIONAL CHRONOLOGY: U.S. Navy (radar), 1941-45; appliance department manager, Oil City Iron Works, 1945-6; student, 1946-52; student engineer in cooperative program with M.I.T., 1948-51; Southwest Research Institute, 1951-(research physicist, department of instrumentation research, 1951-9; manager, electronic instrumentation section 1959-70; staff scientist, 1970-4; institute scientist 1974-).

Memberships: Eta Kappa Nu, Scientific Research Society of America, Sigma Pi Sigma, Institute of Electrical and Electronic Engineers, American Physics Society, Instrument Society of America, and American Society of Agricultural Engineers. Listed in American Men and Women in Science, International Men and Women in Science, Who's Who in the Southwest, and Who's Who in Science. Won the 1987 Imagineer award made by the Mind Science Foundation in San Antonio, The Certificate of Recognition for the creative development of a technical innovation in 1981 for a NASA Tech. Brief entitled "Coal Thickness Gauge Using RRAS Techniques," and the Swearingen Award at SwRI in 1954 for "Low-Frequency Measurements with NMR."

Rev May/88

END

DATE
FILMED
2/19/92